KUOPION YLIOPISTON JULKAISUJA C. LUONNONTIETEET JA YMPÄRISTÖTIETEET 228
KUOPIO UNIVERSITY PUBLICATIONS C. NATURAL AND ENVIRONMENTAL SCIENCES 228

DMITRY SEMENOV

Distance Sensing with Dynamic Speckles

Doctoral dissertation

To be presented by permission of the Faculty of Natural and Environmental Sciences of the University of Kuopio for public examination in Auditorium L3, Canthia building, University of Kuopio, on Friday 14th March 2008, at 12 noon

Department of Physics
University of Kuopio

KUOPION YLIOPISTO

KUOPIO 2008

Distributor: Kuopio University Library
P.O. Box 1627
FI-70211 KUOPIO
FINLAND
Tel. +358 17 163 430
Fax +358 17 163 410
http://www.uku.fi/kirjasto/julkaisutoiminta/julkmyyn.html

Series Editors: Professor Pertti Pasanen, Ph.D.
Department of Environmental Science

Professor Jari Kaipio, Ph.D.
Department of Physics

Author's address: Department of Physics
University of Kuopio
P.O. Box 1627
FI-70211 KUOPIO
FINLAND
Tel. +358 46 8107035
E-mail: dsemenov@uku.fi, dmsemenov@yandex.ru

Supervisors: Professor Alexei Kamshilin, Dr.Sc.
Department of Physics
University of Kuopio

Professor Jari Hämäläinen, Ph.D.
Department of Physics
University of Kuopio

Reviewers: Professor Yoshihisa Aizu, Dr. Eng.
Department of Mechanical Systems Engineering
Muroran Institute of Technology, Japan

Professor Vitrik Oleg Borisovich, Dr.Sc. in Physics
Head of Physics Department,
Far-Eastern National Technical University
Vladivostok, Russia

Opponent: Steen G. Hanson, Ph.D.
Optics and Plasma Research Department,
Riso National Laboratory
Technical University of Denmark
Denmark

ISBN 978-951-27-0966-3
ISBN 978-951-27-1081-2 (PDF)
ISSN 1235-0486

Kopijyvä
Kuopio 2008
Finland

Semenov, Dmitry. Distance sensing with dynamic speckles. Kuopio University Publications C. Natural and Environmental Sciences 228. 2008. 63 p.
ISBN 978-951-27-0966-3
ISBN 978-951-27-1081-2 (PDF)
ISSN 1235-0486

ABSTRACT

In this thesis the technique for measuring distances in the range of several centimetres with micron accuracy and a millisecond response time is presented. The measurements can be made on most optically rough surfaces such as metals, plastics, papers etc. The advantages of the technique are (i) a short response time which makes it possible to work with fast-moving objects, and (ii) the possibility of making measurements on extremely rough surfaces where other sensors such as, for example, triangulation [1] do not reach the required performance.

The proposed technique is based on the well-known speckle effect discovered in the 1960s. Since that time it has been known that moving objects illuminated with a laser produce dynamic speckles [2,3]. Basically the dynamic speckle velocity at the observation plane depends on the distance between the laser and the object surface [4]. This provides an opportunity to build a simple profiler, as speckle velocity can be easily measured using the technique of spatial filtering [5]. However, the speckle method was also known to provide highly dispersed measurement results due to the stochastic nature of speckles. Consequently, dynamic speckle distance measurements were known to provide quite low accuracy, which is not satisfactory for industrial applications.

In this thesis it is demonstrated that object velocity is a key point in improving dynamic speckle method performance. The high velocity of the illuminating beam over the object surface results in an appreciable decrease in the response time of the method. The short response time allows the accumulating and averaging of data, thus greatly improving accuracy. Since most objects in typical industrial applications are quite slow (< 1 m/s) or even static, it was suggested that scanning over the surface of the object should be used. Scanning techniques are well developed and allow velocities of hundreds of meters per second to be achieved. Thus the response time becomes very short and averaging over many scans can be done. Scanning not only improves the performance of the method but also makes it possible to use it with static objects.

It was also found, however, that scanning over a static object produces correlated measurement series. The analysis of spatially filtered dynamic speckles revealed the way to optimize sensor performance. It was shown that the scanning rate should be kept in line with the velocity of the moving object. The analysis of spatially filtered dynamic speckles also suggested an easy way to improve speckle sensing by using many-channel spatial filtering.

Finally, the speckle distance sensor prototype was tested with industrial objects in a manufacturing environment, and performance suitable for industrial applications was demonstrated.

The results of this research are presented in five original papers and one submitted manuscript. Paper **I** demonstrates velocity-independent dynamic speckle measurements using two spatial filters simultaneously. However, this method still depends on the object motion, since the sensor is idle if the object stops. To make measurements completely independent of the motion of the test object, it was decided to generate dynamic speckles by scanning over the object surface. Papers **II-V** study and compare various scanners for a dynamic speckle sensor. The analysis in papers **II-V** makes it possible to choose the most efficient scanner and optimal geometry of the speckle sensor to achieve the highest performance. Paper **V** analyses the correlation properties of dynamic speckles generated with a scanning beam, as these properties differ from the statistical properties of speckles generated with a moving surface.

PACS Classification: 06.30.Bp, 07.07.Df, 42.30.Ms, 42.62.Eh, 42.79.Ls, 81.70.Fy
Universal Decimal Classification: 531.715, 531.719.2, 535.41, 681.586.5, 681.786
INSPEC Thesaurus: distance measurement; optical sensors; lasers; measurement by laser beam; surface measurement; speckle; rough surfaces; optical scanners; acousto-optical deflectors; spatial filters

ACKNOWLEDGMENTS

This study was carried out at the Department of Physics, University of Kuopio, during 2004-2007. The study was supported by the Academy of Finland under project number 107554.

I wish to express my gratitude to my supervisor, Prof. Alexei Kamshilin, for his professional guidance in this research field, for his inspiration and encouragement when I thought that the research has come to a dead end.

I would like to take opportunity to thank Dr. Ervin Nippolainen, whose professionalism and experience in optics greatly improved the results and quality of my research.

I would like to thank Dr. Serguei Miridonov for helpful discussions and suggestions leading to my understanding the nature of the spatially filtered speckle correlation phenomenon.

I am also indebted to all the staff of the Department of Physics with whom I have been in contact, and to many others at the University of Kuopio for rendering help and providing a positive working environment.

LIST OF ABBREVIATIONS AND NOTATIONS

AOD -acousto-optic deflector
DFT- Digital Fourier Transforms
IFE - instant frequency estimation
FFT - Fast Fourier Transforms
IFE - instant frequency estimation
LDV – laser Doppler velocimetry
SDS - speckle distance sensor
SF - spatial filtering
SFV - spatial filtering velocimetry
SNR - signal to noise ratio
PMS - polygonal mirror scanner
TOF - time of flight

η - ratio of translation/boiling regime
r_T - speckle translation length
r_S - average speckle radius
D_S - distance between illumination and observation points
R_W - illuminating beam wave-front curvature in object plane
r_B - radius of the spot on the object
λ - wave length (of illuminating beam)
V_{SP} - speckle velocity
V_{OS} - object surface velocity
V_{LB} - scanning laser beam velocity in respect to the surface
z - distance to the object surface
D_o - distance form observer to the beam waist position.
Z_R - Rayleigh range
Λ - pitch of spatial filter (period)
ε_f - the relative inaccuracy of frequency measurements
ε_z - relative measurement inaccuracy of distance measurements
w_O - beam waist

LIST OF ORIGINAL PUBLICATIONS

The thesis includes the conducted research review based on the peer-reviewed original papers written by the author and devoted to the research field. The original papers are referred to by their Roman numerals:

I. D.V Semenov, E. Nippolainen, and A.A. Kamshilin, "Fast Distance Measurements using Dynamic Speckles," *Optic Letters*, **30**, 248-250 (2005).

II. E. Nippolainen, D.V. Semenov, and A.A. Kamshilin, "Dynamic Speckle Effect Induced by Acousto-Optic Deflector for Fast Range Sensing," *Optic Letters*, **30, pp.** 3147-49 (2005).

III. D.V. Semenov, E. Nippolainen, and A.A. Kamshilin, "Accuracy and resolution of dynamic-speckle profilometer," *Applied Optics*, **45**, pp. 411-418 (2006).

IV. D.V. Semenov, E. Nippolainen, A.A. Kamshilin, A.V. Belyaev, S.V. Andreev, and B.S. Gurevich, " An ultra-fast distance sensor based on dynamic speckles generated by acousto-optic deflection," *Measurement Science and Technology*, **17**, pp. 2906–2912 (2006).

V. D.V Semenov, E. Nippolainen, and A.A. Kamshilin, "Comparison of acousto-optic deflectors for dynamic-speckle distance-measurement application," *Journal of Optics A: Pure and Applied Optics*, **9**, pp. 1-5 (2007).

VI. D.V. Semenov, S. V. Miridonov, E. Nippolainen, and A. A. Kamshilin, "Statistical properties of dynamic speckles formed by a deflecting laser beam," *Optics Express*, **16**, pp. 1238-1249 (2008)

 The thesis contains also previously unpublished data.

CONTENTS

CHAPTER I

1 Introduction

Distance (along with time) is one of the most important features of our world, reflecting the essence of the space-time continuum. In animated nature even before the arrival of homo sapiens, distance and size were central concerns in the successful evolution and survival of living beings in a hostile environment. With the advent of homo sapiens, the measurement of distance became rational. For tens of thousands of years of human existence, the prosperity of mankind has required increasingly sophisticated measuring devices and techniques. Nowadays human beings operate with extremely wide ranges of distances, from the size of the visible universe ($\sim 10^{26}$ m) down to the subatomic range ($\sim 10^{-14}$ m) and even less. Of course, there is no universal measuring device for such a wide distance range and each range refers to some particular method and is limited by a given interval. In this way distance measuring methods vary from basic manual techniques to sophisticated automatic controls and even indirect theoretical estimations. Due to the increasing acceleration of the pace of modern life, human activities require faster and more accurate distance measuring devices for determining position on the earth's surface, for navigation in space, for microscopy, and, of course, for industrial applications. The requirements for industrial sensors are increasing with the speed of technological progress - machines become faster, more intelligent; quality of control systems and manufacturing tolerances become stricter in terms of accuracy. Thus, more accurate sensors are needed.

This thesis is devoted to the measurement of the distance to an optically rough surface in the range of several centimetres. The accuracy of the measurement depends on the measuring window. In the case of a single channel sensor (single photo-receiver), micron accuracy is achieved within several milliseconds. A short response time is a very important parameter of any sensor. Objects in industrial environments are moving sometimes with extremely high velocities: in paper lines, for example, it is tens of meters per second, while an accuracy of microns is required. It is clear that with a slow sensor the displacement of the object during measurement will greatly reduce lateral resolution. At the same time micron accuracy usually requires some averaging (long measuring window), which means that the measurement process is not as fast as desired. This is quite a challenging task for any sensor. However, the speckle sensor considered here is able to complete measurements within microseconds, depending on the required accuracy. For a 1 ms measuring window, the displacement of an object moving with a velocity of 10 m/s is equal to 10 mm, which can be considered a "good" result.

The other advantage of the proposed sensor is the possibility to work with optically rough surfaces. Usually surfaces which produce high scattering reduce the accuracy of measurements. For triangulation sensors this is because of the speckle effect when using a laser or a not well-defined reflected beam profile for a non-coherent light source. For contact sensors that is impossibility to achieve accuracy higher then the object roughness and slow response (< 1 kHz) when the surface roughness is high. In contrast, a speckle sensor does not work with specular surfaces, while with rough objects its performance is sometimes higher than with other techniques. As rough surfaces are more common than specular ones in industrial environments, the speckle sensor can find a wide area of applications.

In addition to the above-mentioned abilities to work with fast-moving objects and to provide measurements on rough surfaces, another advantage of the speckle sensor is that it does not involve any sophisticated expensive mechanics, optics or electronics. Basically the sensor measures the dynamic speckle velocity generated by a moving object illuminated with a laser. In this case speckle velocity is a function of the

distance between the optical head (laser) and the object surface [3,6]. Spatial filtering [5,7] allows fast measurement of speckle velocity: a speckle moving across a periodic transmittance (e.g. simple diffraction grating) produces light power modulation behind the transmittance, whose frequency is directly proportional to the velocity of the speckles. Modulation frequency can be measured using any common frequency measurement technique (zero-crossing, Fast Fourier Transforms etc.), and the frequency value represents speckle velocity and therefore z-distance.

The technique described in this thesis is optical and therefore non-contact, which is preferable in modern industry. The method of measurements is original, and to the best of the author's knowledge no sensor of this type has been applied in industrial environment so far. Due to its rather simple construction and high performance, it is expected that the speckle distance sensor will replace the outdated devices which are currently in use in some industrial applications.

CHAPTER II

2 The aims and contents of the thesis

The aim of this thesis is to propose a novel method for distance measurement in the 0.1 - 50 mm measuring range with micron accuracy. One of the targets of proposed method is measuring the thickness of spray coatings. The spray coatings are widely used to provide thermal, corrosion and other protection for different surfaces. The thickness of coating is typically within several hundred of microns while required accuracy of coating thickness is of microns. The control of spray coating must be realized in real time during deposition and the duration of deposition is typically very short (several seconds). Due to the beating (object is typically rotating while the coating is sprayed on the object) and thermal expansion of the object (high temperature of plasma jet) the position of the target surface can vary within several millimetres. Thus coating thickness measurement is quite challenging task for any conventional sensor and no universal solution was found yet. In this thesis the performance of proposed method is demonstrated by the example of protective coating. The other anticipated examples of proposed technique applications are rolled metal thickness measurement, weld seam inspections, online measurement of paper-web thickness, profile monitoring of fast-rotating rolls and reels in papermaking machine, to mention a few.
The proposed method exploits dynamic speckles; for this reason, throughout the thesis the prototype of the distance sensor is called a *Speckle Distance Sensor (SDS)* or *speckle sensor* or simply *sensor*. The distinguishing features of a SDS are

- non-contact operation mode
- applicability to most optically rough surfaces
- short response time (μs)
- capability to work with fast-moving surfaces
- simple optic and electronic construction

The method is optical and therefore non-contact. Non-contact measurements are preferable in most cases, as contact sensors are usually subjected to deterioration. This decreases accuracy with time and some contacting parts of such sensors must be replaced sooner or later, which means that the manufacturing process has to be stopped for maintenance inspections occasionally. Moreover, in some cases contact measurements are impossible or can be accomplished only with great difficulty due to certain manufacturing factors:

- aggressive media (high temperature etc.)
- scratch-sensitive components
- soft or easily deformable components (paper etc.)
- contact measurements with accuracy higher than object roughness

The most remarkable feature of the technique is the response time, which can be extremely short. The shortest response time in distance-estimating experiments was just 12 ns. However, such short response time does not provide acceptable accuracy. To increase accuracy, averaging over a series of measurements is needed. To get acceptable accuracy after averaging, the total response time was increased up to several microseconds.

The proposed method works with most optically rough surfaces (metals, plastic, papers etc.). The best results were obtained with strongly scattering surfaces without light penetration into the media, such as metals. Nevertheless, the method also works with paper but then the response time is longer. Some conventional

methods do not work with very rough surfaces especially when the required accuracy is higher than the roughness of the surface. The speckle sensor copes perfectly with the task, as the rough surface is an integral part of the measurement.

The other advantage of the proposed method is the possibility to work with rapidly moving surfaces due to the short response time of the sensor. Various applications of speckle metrology also involve object velocity measurement [8,9,10]. Fast-moving surfaces are an integral part of many industrial processes. Let us consider a production line continuously moving with a velocity of 10 meters per second. In this case, to achieve a resolution of 1 cm along the surface motion direction, the measurement time should be reduced to just 1 ms. Achieving an accuracy of microns in such a short time is really challenging for both contact and non-contact techniques.

The other distinguishing feature of the technique is a simple optical and electronic arrangement, which results in a relatively low cost of the final product. Simple optics means that no expensive multi-lens objectives are needed. Conventional thin lenses are adequate to ensure high performance of the sensor. Simple electronics mean that the device is quite inexpensive but it is still capable of working in real time with a response time of microseconds.

CHAPTER III

3 Review of alternative measurement techniques

As a result of ever shorter production cycles, the demand for industrial metrology increase simultaneously with the demands on manufacturing quality. Estimating the distance to objects, acquiring information about object profiles and object surfaces, and 3D vision applications require fast, robust, and accurate solutions. Current methods can be divided into two main categories: touch mechanical and non-contact sensing. Contact measurements have obvious disadvantages: a long response time, deterioration, and required constant contact with a surface. There are also more advanced technologies based on non-contact principles, including several techniques based on various physical phenomena: electromagnetism, acoustics, and optics. In this review some basic details of mechanical probes and non-optical techniques are given, and then a more detailed description of optical distance sensing principles and their advantages and disadvantages are provided.

3.1 Conventional contact measurements

Conventional touch range sensors are based on a touch trigger probe installed in a coordinate measuring machine [11]. The end of the probe stem is deflected by the contact surface thus producing a corresponding step voltage, which indicates instant position. Such probes are well developed and have excellent accuracy and repeatability. However, the application of touch probes is limited. Due to the need for mechanical contact with a surface, touch probes require careful surface contact and therefore they are quite slow (~ 1 kHz). A low measurement frequency makes it impossible to make measurements with fast-moving objects. The other problem is the measurement of the surface profile when the roughness of the surface is comparable to or higher than the profile variation. In this case, due to the need for uninterrupted contact with the object, fast accurate measurements are impossible.

3.2 Non-optical contactless sensors

Typical non-optical contactless range sensors use electromagnetic and acoustic phenomena. Inductive sensors and capacitive sensors are referred to as field-based sensors [12,13,14]. Inductive sensors are limited only by measuring distance to metallic surfaces. Capacitive sensors can be activated with either conductive or non-conductive materials but the sensor cannot work with several different materials simultaneously. The typical sensing range of field-based sensors is the same as that of the speckle sensor (within 5-20 mm); however, field-based sensors are not accurate and usually are used as presence sensors. Besides, field-based sensors are strongly affected by environmental conditions such as humidity, dust etc.

Acoustic [13,15] methods are referred to as the time-of-flight technique and are described below in section 3.3.1. The disadvantage of such methods is low resolution in the *x*-*y* plane, which is defined by the acoustic beam diameter.

3.3 Optical methods

The main advantages of optical measurements [16] are the absence of direct contact with the test product and the possibility of making measurements extremely fast. Many optical measurement methods are still in the research stage. Optical techniques can be divided into several independent groups: geometric (triangulation, auto-focus, image processing), time-of-flight, interferometry, diffraction. Optical methods are preferable because of their rapidity and the absence of physical contact with the test objects.

3.3.1 Time-of-flight

The time-of-flight (TOF) method [17] measures the signal carrier (acoustic or electromagnetic waves) travel time, assuming that the propagation velocity is known. Typically, an observer emits a signal; the signal is reflected from the object and comes back, while the observer registers the total travelling time. TOF ranging using light is known as LIDAR (light detection and ranging) [17]. Using a laser is preferable as a laser is capable of producing very narrow beams to get accurate resolution in the *x*-*y* plane. The main problem is that improving *z*-accuracy requires measuring very short time intervals because of the extremely high velocity of the light. To operate with even 1 m length, measurement of one billionths of a second is needed. TOF using acoustics is much more precise in the *z*-coordinate. However, it is much more difficult to concentrate the sound energy into a narrow beam to get high *x*-*y* resolution.

3.3.2 Interferometry

The interaction of two coherent beams leads to interference and light intensity variation at the observation plane. If one beam is the reference beam and the other is sent to the object and reflected back, then the position of the fringes in the interference picture depends on the distance to the object, which defines the phase difference between the reference and the object beams. Interferometric range measurements are divided into modulated and unmodulated [18]. The unmodulated technique uses only one wave length for measurement, so the measurements interval is limited as light intensity alternation is a periodic function of the *z*-distance with the period equal to the wavelength. However, it can be an extremely accurate tool, with a resolution of 0.01 μm.

Using modulated light makes it possible to increase the range. The output signal in the case of modulated interferometry is also a periodic function of the object range. However, the period now is equal to the modulation wavelength, which is under the experimenter's control. These wavelengths can be long. Thus, high resolution range measurements require very high resolution phase measurement of the modulated signal returning from the object. This, in turn, requires time averaging over many periods of modulation. Thus, there is a direct trade-off in range resolution and temporal resolution. In spite of the available longer measurement range, interferometric measurements [19] are quite a challenging problem especially if the surface is very rough and moving.

3.3.3 Triangulation

Triangulation has become a standard method for distance measurement. In the SDS application field it is the most advanced and most investigated of the optical distance measurement techniques [20], and it can be considered to be the main competitor of the dynamic speckle sensor. Triangulation utilizes the basic geometrical properties of a triangle, enabling calculation of the other sides of the triangle when the base of the triangle is known and the adjacent angles are measured. Measuring the angles implies object observation from two different points. It can be either measurement of displacement of an image point from a reference point in the detector plane (active: point projection, grids projection techniques etc.) or the acquisition of two images (passive: stereo imaging).

Triangulation has evident advantages:

- simple concept, easy and straightforward to implement
- easy to scale over a large range

But there are also disadvantages:

- a generic problem with triangulation techniques is missing data. As the object is being viewed from at least two perspectives, there can be points which are visible in only one of the views

- non-specular surfaces complicate the measurement due to irregularly scattered light. Rough surfaces noticeably reduce the accuracy of defused light detection
- both the passive and the active triangulation techniques are resource-intensive from the data processing point of view.

These last two disadvantages of triangulations can be overcome by the dynamic speckle sensor, which thus fills a niche in the distance measurement field.

3.3.4 Diffraction-based techniques

Diffraction techniques are based on the scattering of coherent light in an inhomogeneous medium. If a spot on a test object is coherently illuminated, the scattered light will form a speckle pattern on a screen (at the observation plane). The properties of the speckle pattern depend on the distance between the test object and the screen. For example, measuring the speckle pattern correlation length provides information about the distance [21,22,23].

The main advantage of speckle metrology is the speed of data acquisition. For the previously discussed systems, kilohertz data rates are difficult to obtain and the measurement process is generally much slower. With a speckle approach, the entire field of interest is illuminated in parallel and can be viewed with a video camera, for example. A simple analogue filter is used to measure the fringe contrast on the video signal; thus, megahertz data rates are achieved. In a SDS, the function of narrow-band-pass filter is realized by means of periodic transmittance (spatial filter). Due to the modulation effect which periodic transmittance has upon dynamic speckles, the intensity of the light passing through the spatial filter is modulated at a frequency proportional to the velocity of the speckles. Using spatial filtering and taking into account the very high speckle velocity generated in a SDS by means of scanning, a modulation frequency of 80 MHz was achieved. Thus, the response time of a SDS can be as short as 12 ns.

3.4 Conclusion

In comparison with other optical methods, the speckle distance sensor has incontestable advantages in its particular measurements range. In contrast to TOF and interferometry techniques, the SDS satisfies all these requirements at once: a high dynamic range (1,000:1), micron z-accuracy, sub-millimetre x-y resolution, and a short response time. Together with being able to work with fast-moving rough surfaces, the above- mentioned parameters of a SDS are very promising. In some fields, especially concerning strongly scattering surfaces, the SDS is far better than any other range technique. For example, in the case of as-deposited protective coatings, the coating thickness control often fails to operate in real-time when using conventional methods. As for triangulation, which can be considered to be the main competitor of the SDS sensor, the dynamic speckles method has the advantages of rapidity and being independent of object roughness. Comparing a dynamic speckles sensor with a triangulation sensor, we see that:

- both the SDS and triangulation are very simple and straightforward to implement
- the response time of the SDS is extremely short (~ 12 ns)
- the range of the SDS cannot be extended to meters. However, in its particular range the speckle sensor is much faster than any other method
- data missing due to a rapidly changing surface profile is a challenge to both the speckle sensor and the triangulation sensor. However, in some cases the speckle sensor can easily measure even abruptly changing profiles (see a profile measured with a double-face mirror sensor in **paper III**)
- a diffused object surface is an integral part of the measurement process. The speckle sensor works with metals, plastics, and papers. While it cannot work with any specular objects, the SDS still has a wide application field since diffused objects are typical in industrial environments.

- the only resource-intensive procedure in data processing using the SDS could be frequency measurements (1-100 MHz) in real time. However, frequency measurement techniques are well-established, e.g. using the zero-crossing technique one can measure frequency in real time even without advanced electronics.

Thus one can see that the speckle distance sensor is faster in its application field than touch range sensors and other optical techniques, making it possible to work with fast-moving objects (tens m/s), which is difficult with other methods. Usually the accuracy of range measurement techniques diminishes when measuring on a rough surface. The most developed triangulation method reduces the response time because of speckle effect when measurement is applied to the rough objects. In its turn, the SDS uses the speckle effect and requires a rough surface for making measurements.

The scanning speckle sensor does not involve any sophisticated optics, mechanics or electronics. State-of-the-art scanning techniques are widely using in commercial products, from laser jet printers to bar-code readers. The optics and electronics of the SDS do not require any expensive solution: a simple semiconductor laser, several spherical lenses, basic grating for spatial filtering, and conventional counting electronics for frequency measurements. This means that the production cost of the industrial sensor can be very competitive.

Measuring in the centimetre range with micron accuracy is quite a common industrial task (material production, evaporating thin films and spraying on protective coatings, surface deterioration detection etc.) and this is the purpose of the speckle distance sensor. Rough surfaces are common in the ambient environment and also in industry. Fast-moving surfaces are common in many industrial processes. Velocities are continuously increasing, reaching tens of m/s and demanding very high measuring rates.

In this thesis it will be demonstrated that the speckle sensor satisfies all those strict requirements in its particular range. Considering the quite simple arrangement of the SDS and the prevalence of rough as opposed to specular surfaces in the ambient environment, it is shown that the SDS can be used in many applications where it will be more competitive than other methods, or where other methods do not work at all.

CHAPTER IV

4 Review of speckle-based distance measurements

4.1 Speckles and their application in distance measurement

Speckle patterns, or speckles, are known as a random intensity light patterns produced by a coherent wavefront scattered in an inhomogeneous medium [24]. However, speckle patterns can be produced by any other coherent wave processes such as interference of other electromagnetic spectrum waves or acoustic waves or even the waves on the surface of water. One well-known example of visible light speckle patterns are the highly magnified images of a star seen through imperfect optics or through the atmosphere. Another example, relevant directly to this thesis, is the random intensity light pattern created by a laser beam reflected off an optically rough surface. The speckle patterns considered in the thesis are generated with visible and near infrared light; however, other wavelengths are also allowable. The typical speckle patterns are shown in Fig. 4.1(a,b).

When the illuminated surface undergoes displacement or any deformation, the speckle structure shows changes as well. If the speckle pattern is produced by visible light, then the displacement of speckles can be easily observed even with the naked eye everywhere in space. The changes in the speckle pattern contain information about the object displacement and deformation. The speckle pattern properties are determined by the distance to the point of observation from the object surface, the illuminating beam numerical aperture, and the diameter of the illuminating spot on the object surface. Using this knowledge and analysing the behaviour of speckles, one can obtain such information as the direction of the scattering object motion, its velocity, and distance to the object.

Speckle displacement can be quantitatively represented as the displacement of the peak position of the cross-correlation function of the light intensity distribution before and after the object was moved [25]. Fig. 4.1 shows two speckle patterns before (Fig. 4.1(a)) and after (Fig. 4.1(b)) in-plane translation of an object and respective 2-dimensional auto-correlation (Fig. 4.1(c)) and cross-correlation functions (Fig. 4.1(d)).

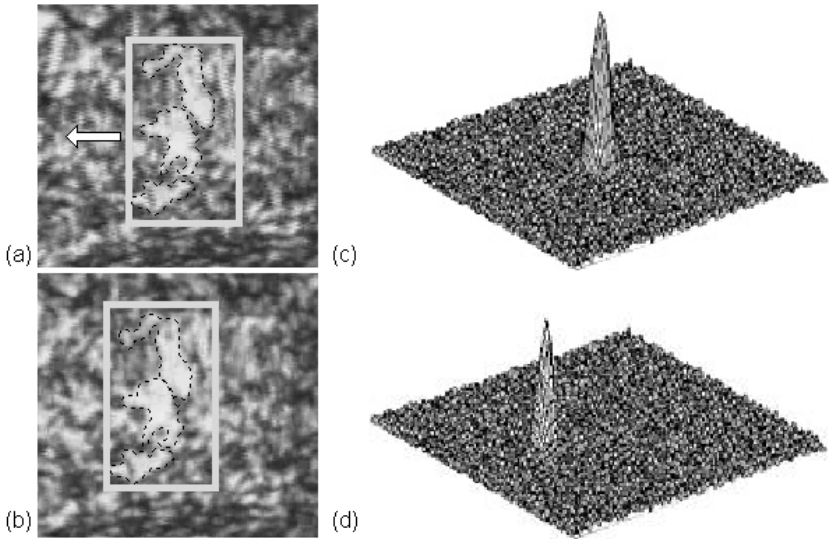

Figure 4.1 Speckle pattern at the image plane before (a) and after (b) object displacement. Speckles which preserved their shape after displacement are marked with a dash line. Autocorrelation and cross-correlation functions are shown in (c) and (d).

As the auto-correlation peak is always located at zero, the peak position of the cross-correlation function in general deviates from zero, see Fig. 4.1(d). This deviation of the peak corresponds to speckle displacement, while the change of peak height (see Fig. 4.1(d)) is referred to as decorrelation of speckles or the change in speckle pattern structure after displacement. Speckle displacement and decorrelation are caused by the random summation of phases of interfering waves. The phase change results from variation in the optical paths of many scattered waves from a rough object surface.

Since speckle displacement is proportional to the amount of object deformation / translation, speckles can be used for random marking of the surface. Detection of speckle displacement / speckle velocity is a key point of speckle measurement. Speckle displacement detection methods include various techniques, which are discussed in detail in many sources: speckle photography [26,27,28], the one-dimensional speckle correlation method [29,21] and spatial filtering [5]. The latter method, spatial filtering, was developed mainly for small particle velocity measurement, and this method is also used in the SDS for speckle velocity measurement.

The parameters of a speckle pattern and its behaviour strongly depend on the numerical aperture and diameter of the illuminating beam, the wavefront curvature at the object plane, and observer location. Speckle motion can be categorized as boiling and translation motion. In boiling motion the speckles change their shape and size with the motion of the object. Translation speckle motion is related to motion of the speckle pattern as a whole. In pure boiling motion there is no point in defining speckle displacement. Usually in arbitrary conditions there is no pure boiling or translation motion of speckles, but a mixture of both. The translation/boiling regime of speckle motion is defined as a ratio of the translation distance, r_T, to the average speckle radius, r_S [30]:

$$\eta = \frac{r_T}{r_S} \qquad (4.1)$$

where

$$r_T = (1 + \frac{D_S}{R_W}) \cdot r_B \qquad (4.2)$$

$$r_S = \frac{D_S \cdot \lambda}{\pi \cdot r_B} \qquad (4.3)$$

Here the translation distance, r_T, is calculated for the illumination with a Gaussian beam [30]; D_S is the distance between the illumination and observation point; R_W is the illuminating beam wave-front curvature at the object plane; r_B is the radius of the spot on the object; λ is a wavelength generated with a laser.

According to Eq. 4.1 if $\eta = 0$, the dynamic speckles show pure boiling; if $|\eta| < 1$, boiling becomes dominant; if $|\eta| > 1$, translation becomes dominant. Using this factor η, one can evaluate two types of motion of dynamic speckles.

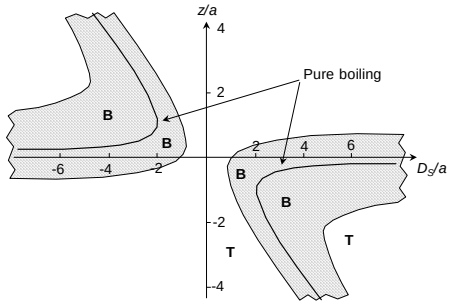

Figure 4.2. The type of motion of dynamic speckles under Gaussian-beam illumination as a function of object position z and position of the observer D_S. The symbols B and T indicate the boiling and translation regions, respectively, of the speckle motion. Here $a = \pi w_o^2/\lambda$; w_o - beam radius at the beam waist position.

For distance and velocity measurements, which use dynamic speckles, translation motion must be predominant. In the thesis, only illumination of the object with the Gaussian beam using a simple convex lens to focus the laser beam in TEM_{00} mode is considered. The speckle motion regime should be chosen in accordance with the diagram in Fig. 4.2. Here the solid lines indicate pure boiling motion of speckles and shaded areas around the solid lines refer to predominance of boiling motion. Unshaded part of the figure refers to predominance of translation speckle motion. In the case of the divergent / convergent illuminating beam, the speckle displacement is directly proportional to the displacement of the object and inversely proportional to the distance between the beam-waist position and the object surface, z [3]. The displacements can be easily transferred to velocities and thus the dependence of speckle velocity on the object in-plane motion velocity and z-coordinate can be expressed by a simple equation [3]:

$$V_{SP}(z) = V_{OS}\left[1 + \frac{D_S(z)}{R_W(z)}\right] \qquad (4.4)$$

Here, V_{SP} is the speckle velocity, V_{OS} is the object surface velocity. Both $D_S(z)$ and $R_W(z)$ are functions of the z-distance.

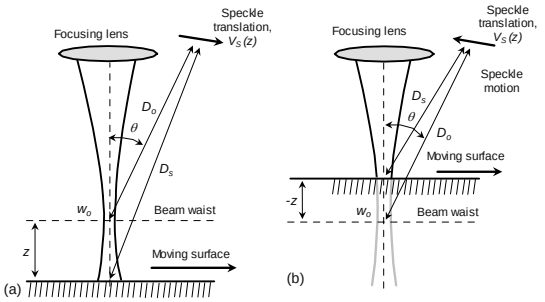

Figure 4.3. Principle of z-distance measurement or object velocity measurement using dynamic speckles in divergent (a) and convergent (b) illuminating-beam configurations. In both cases the wavefront curvature R_W is a function of z-distance from the beam waist position, and the wavefront curvature defines the speckles velocity $V_S(z)$ at the observation plane according to Eq. 4.4.

For translation speckle motion one can define the velocity, V_{SP}, which is a function of the object surface velocity, V_{OS}, and the geometry of the experiment. The geometry includes the distance between the points of observation and illumination, D_S, and the wavefront curvature of the illuminating beam, R_W. The wave front curvature is implied to be much larger than the curvature of the object surface within the illuminated area.
Here the wavefront radius R_W is measured from the position of the waist of the illuminating focused beam denoted by z. For the illuminating beam of the Gaussian TEM_{00} mode, the wavefront radius is equal to the distance z when z is larger than the Rayleigh range, $z >> Z_R = \pi w_0^2 / \lambda$. The object under study can be located either after beam waist position as shown in Fig. 4.3(a) or between the beam waist position and focusing lens as shown in Fig. 4.3(b). In both cases according to Eq. 4.4 the speckle pattern velocity represents the z-distance to the object surface, if the object surface velocity V_{OS} is known. Thus at a constant object velocity the distance to the object surface can easily be calculated if speckle velocity is measured, and to measure speckle velocity, the simplest and fastest spatial filtering technique is utilized.

4.2 Spatial filtering

A spatial filtering method is an integral part of the SDS. Spatial filtering has been attracting the interest of many researchers since the 1960s, when lasers were developed and various novel optical measuring methods were introduced. Spatial filtering is quite a simple alternative to Laser Doppler Velocimetry (LDV), which allows non-contact measuring of the velocity of moving objects, images, small particles in air and water flows, and laser speckles. The first definite mention of spatial filtering (SF) was made in 1963 in [31], where the operation of a parallel-slit reticle was simulated. The first experimental demonstration of SF for fluid flow velocity measurements is given in [32]. The SF technique has been developing since then, many experimental data have been collected and many theoretical backgrounds have evolved. In 2006 the book "Spatial Filtering Velocimetry" by Y. Aizu et al.[5] was published. The book covers all the aspects of SF including principles and properties, optical setup, signal analysing, and applications. This thesis refers to this book very often. However, the book is mainly devoted to object velocity measurement. The thesis presents some new properties of spatial filtering from the point of view of distance measurement (see **paper VI**), which, to the best of the author's knowledge, have not been presented previously.

The principle of spatial filtering velocimetry (SFV) is based on the light intensity modulation caused by an image moving through the periodic transmittance. Fig. 4.4 shows the basic operation of SFV. Here the moving object is represented by a number of small particles moving in one direction. The image formed by a lens of each small particle is moving with constant velocity, v_o, in the direction x_o perpendicular to the slits of a spatial filter (here the SF is a sequence of light-transmitting and -blocking strips). The light passed through the spatial filter is received by the photodetector. The total intensity of detected light varies periodically because the image moves with constant velocity, v_o, perpendicular to the periodic transmittance having a

period Λ (spatial period), see Fig. 4.4. Thus the output from the photodetector provides a periodic signal containing period $T_o = \Lambda / v_o$. By measuring the frequency $f_o = 1 / T_o$ of modulated signal, one can find the velocity of particles as $\upsilon_o \sim \frac{\Lambda}{M} \cdot f_o$, where M is the optical magnification of the imaging system with the lens.

The same process takes place when speckles are moving across a spatial filter in free space. In this case no optics for magnification is used and, as M=1, the speckle velocity, V_{SP}, is simply determined as

$$V_{SP} \sim \Lambda \cdot f_o \qquad (4.5)$$

where f_o is the frequency of the modulated photocurrent.

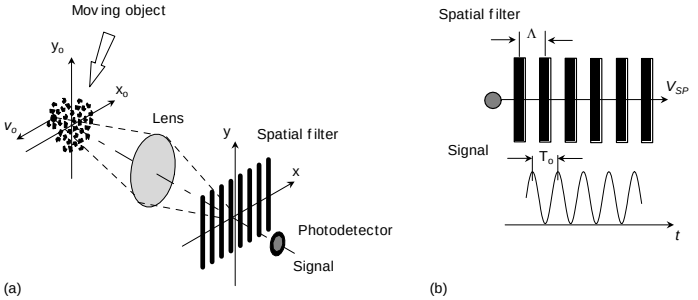

Figure 4.4 (a) Basic optical system of spatial filtering velocimetry, (b) spatial filter response to moving image.

In this way by combining Eq. 4.5 and Eq. 4.4 the main equation for distance speckle sensor is derived [4,30,7]:

$$f_{SP}(z) = \frac{V_{OS}}{\Lambda}\left[1 + \frac{D_S(z)}{R_W(z)}\right] \qquad (4.6)$$

Remembering that out of the Rayleigh range the wavefront radius is equal to the distance from the beam waist position to the object surface, one can easily calculate this z-distance assuming that $D_S \sim D_o + z$, where D_o is the distance form the observer to the beam waist position. If the modulation frequency is measured then the relationship between f_{SP} and z-distance is as follows:

$$f_{SP}(z) = \frac{V_{OS}}{\Lambda}\left[2 + \frac{D_o}{z}\right] \qquad (4.7)$$

Equations 4.6 and 4.7 are valid for moving surfaces and static laser beams. The main part of the thesis is devoted to a scanning laser beam. If the laser beam moves with velocity V_{LB} in respect to the static observer and the static surface, then both equations 4.6 and 4.7 are slightly changed. In this case speckle velocity in the observer's reference frame, V_{SP}, is smaller by the velocity of the laser beam, $V_{SP} = V'_{SP} - V_{LB}$, here V'_{SP} is the speckle velocity in the laser beam reference frame. The analogue of equations 4.6 and 4.7 for scanning beam are shown below (equations 4.8 and 4.9, respectively):

$$f_{SP}(z) = \frac{V_{LB}}{\Lambda}\frac{D_S(z)}{R_W(z)} \qquad (4.8)$$

$$f_{SP}(z) = \frac{V_{LB}}{\Lambda}\left(1 + \frac{D_o}{z}\right) \qquad (4.9)$$

The position of the spatial filter, D_o, and its spatial period, Λ, can be measured accurately. If the object velocity, V_{OS}, (or scanning velocity, V_{LB}) is known, then the z-distance is completely determined by the measured frequency of the modulated photocurrent. The modulated photocurrent shape is close to sinusoidal. However, the photocurrent has a random amplitude and phase fluctuations due to the stochastic nature of speckles (typical photocurrents are shown in Fig. 4.5(a) and Fig. 4.6). In case of speckle measurements

among other parameters the shape of the photocurrent is defined by the aperture of the SF. The relative spectrum width of the modulated photocurrent for the square profile of the SF is inversely proportional to the number of grating lines within the interval of speckle translation and the total number of grating lines [40]. However, the reasonable size of and profile of the SF for practical measurements is under consideration. For example, as it is shown in this thesis two adjacent spatial filters can produce uncorrelated photocurrents. In this case it is reasonable to use two smaller spatial filters instead of bigger one and average the measurements from two channels. The minimal size of the SF at the same time is defined by the sensitivity of photoreceiver and electronics. As it is demonstrated in this thesis the signal-to-noise ration (SNR) in the photocurrent is strongly depends on the light power collected to the photodiode. Therefore, optimization SF profile and the number of SF require additional study. It is worth noting that spatial filtering can be realized not only by means of grating as it is shown in Fig. 4.4 but also by using an array of optical fibers. The laser speckle velocimeter based on optical fibers is demonstrated in [9]. However, from the signal processing point of view any type of spatial filter results in a narrow band random signal, which central frequency defines the average speckle velocity (and for the SDS also *z*-distance to the object). Proper frequency measurement techniques for this type of signal are described in next section.

4.3 Signal processing techniques

Measurement of the *z*-coordinate in the SDS is indirect: it is done through measurement of the frequency of modulated light power after spatial filtering. To get better accuracy of the *z*-coordinate, the frequency should be measured in an optimal way using appropriate electronic equipment. The modulated signal from the photodetector is non-ideal sinusoid, as was mentioned, but it is a narrow-band random signal sometimes intermittent with no signal intervals or drop-outs. Simple frequency counters or a spectrum analyzer can be used for frequency measurement. However, the accuracy provided with these methods is usually unsatisfactory for real SF signals: low SNR, and drop-outs erroneously processed as informative components strongly impair the accuracy. Fortunately, the type of SF signal is quite similar to that of LDV and some of the signal-analyzing approaches from LDV can be applied to SFV. In this section several signal-analyzing techniques for frequency measurements are considered. The emphasis is placed on the techniques utilized in experiments with distance sensor prototypes. Typical LDV measurement equipment is reviewed in [33,34,35].

A continuous periodic signal is very rare in SF measurements (and with scanning it is certainly discontinuous). Typical oscilloscope traces are shown in Fig. 4.5(a). It can be seen that well-defined modulation is alternated with drop-outs and with periods of low SNR. This is the result of the summation of modulations provided by many speckles on the spatial filter. As was mentioned above, the motion of the speckles cannot be referred only to translation one but simultaneously some boiling component is always included. This means that the shape and size of the speckles vary in time, introducing stochastic noise into the modulation. The phase and amplitude fluctuations bring to resultant spectrum broadening [36]. In Fig. 4.5(b) the photocurrent is simulated by the summation of 10 sinusoidal signals with different periods. Each of the sinusoids in the simulation has a random period, which deviates about 7-10% from the period of the central sinusoid. It can be seen that the shape of the simulated photocurrent has much in common with a real photocurrent acquired with SF. Both signals contain informative bursts, which are intermittent with drop-outs.

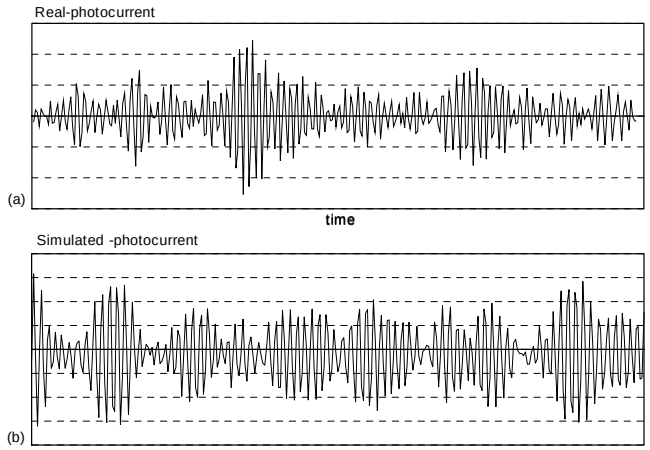

Figure 4.5. a) Real photocurrent, (b) sum of 10 sinusoids with variable periods ($\Delta T/T \sim 10\%$).

Due to the non-continuous nature of the signal, a signal-processing technique, operating only with well-defined modulated intervals, is required to detect dropouts. There are several signal processing techniques which may be chosen for SFV. A review of suitable techniques is given in [5]. These techniques are represented by: spectrum analysis, frequency tracking, and counting techniques.

In the present research the following main methods of frequency estimations were utilized: Fourier transforms (referred to as spectrum analysis), and the zero-crossing method (counting technique). These methods were used in all cases except the estimation of correlations for the longitudinal object displacement in **paper VI**, where the method of instant frequency estimation (IFE) was used for correlation estimations [37]. Fourier transforms realised by means of Fast Fourier Transforms (FFT) [38,39] give the highest accuracy. However, utilization of the MatLAB processing tools box showed that this method cannot compute in real time for frequencies of 10-100 MHz using current personal computers. IFE allows the estimation of the instant value of the frequency and is also resource-intensive. The zero-crossing method is the fastest one. In spite of having the worst accuracy, it gives the best ratio of accuracy/execution time. This method can be easily and cost effectively realized with electronics, so it is the most appropriate technique for this case especially if one takes into account the multi-channel spatial filtering described in **paper VI**. The zero-crossing method was applied not only using digital oscilloscope and MatLAB but also using an electronic frequency-meter (0.1-25 MHz) and was utilized in some experiments for data acquisition using a PC.

In the thesis, the above-mentioned three methods were not studied in respect to speckle measurements from the computational and mathematical points of view because that is beyond the scope of this work. However, such a study would be very interesting. The optimisation of algorithms and the constantly increasing power of electronics make it likely that in the near future the procedure for data processing will be chosen according to the best accuracy and not for electronic processing speed.

4.3.1 Fast Fourier Transforms

The frequency spectrum of a photocurrent can be obtained using the Fourier transform. There are several conventional definitions for the Fourier transform. Here are the formulas accepted in communications and signal processing:

$$S(f) = \int_{-\infty}^{\infty} g(t) \cdot e^{-i2\pi ft} dt \qquad (4.10)$$

$$g(t) = \int_{-\infty}^{\infty} S(f) \cdot e^{i2\pi ft} df\,, \qquad (4.11)$$

where *g(t)* and *S(f)* are the signal function and its Fourier transform, respectively. When the independent variable *t* represents time (with SI unit of seconds), the transform variable *f* represents ordinary frequency (in hertz). The complex-valued function, *S*, is said to represent *g* in the frequency domain. In this case the function $A(f) = |S(f)|$ represents the power spectrum or the amplitude of the harmonic with frequency, *f*, which is the target of the distance sensor measurements. The power spectrum was typically used in the laboratory for fast frequency estimation.

Digital oscilloscope digitises the signal from the photodiode. Therefore utilization of Discrete Fourier Transforms (DFT) is needed. DFT is defined as

$$S_n = \sum_{k=0}^{N-1} g_k \cdot e^{-\frac{2\pi i}{N}nk}\,, \text{ where } n = 0,..., N\text{-}1 \qquad (4.12)$$

$$g_k = \sum_{n=0}^{N-1} S_n \cdot e^{-\frac{2\pi i}{N}nk}\,, \text{ where } k = 0,..., N\text{-}1 \qquad (4.13)$$

Here *n* and *k* are the discrete frequency and time for sampling the spectrum and the signal. *N* is the number of sampling data. If the sampling theorem is satisfied then the discrete spectrum can be a good approximation of the continuous Fourier transform.

The FFT is an efficient algorithm to compute the DFT. Evaluating these sums (see Eq. 4.12) directly would take N^2 multiplications and $N \cdot (N\text{-}1)$ additions with the DFT. An FFT [38] is an algorithm to compute the same result in only $N \cdot log_2 N$ operations.

As was said above, the typical signals in speckle measurements are narrow band random signals and they normally contain a range of harmonics. Due to the stochastic nature of the speckles, the amplitude and phase of modulation are randomly changing. Therefore, Fourier transforms cannot give precise frequency estimations to micron accuracy for short time intervals. The main reason for this is that usually the spectral profile is irregular and can contain not one but two or even more extremums. As the spectral profile is close to the Gaussian shape [40], accuracy improvement requires additional approximation with the Gaussian function $f(x) = a \cdot e^{-(x-b)^2/(2c^2)}$. In this case the position of the centre of the Gaussian function peak represents the sought value of the frequency.

Both operations, FFT and Gaussian approximation, are recourse-intensive procedures. Estimations with MatLAB using a Pentium IV processor show that those operations can hardly be realized in real time for the above-mentioned frequency range. Nevertheless, due to the high accuracy of FFT together with Gaussian approximation they have been used for research purposes very often where time of execution is not important.

4.3.2 Zero-crossing

Zero-crossing is a commonly used term in electronics, mathematics, and image processing. In mathematical terms, it means basically changing of the sign (e.g. from positive to negative), which is represented with a

crossing of the axis (zero-value) in a graph of a particular function. In electronics, the zero crossing for alternating current is the instantaneous point at which there is no voltage present. In a sine wave or other simple waveform, this normally occurs twice during each cycle. The zero-crossing method works perfectly with sinusoidal signals and it can be applied with spatially filtered dynamic speckles [41]. However, in the case of the speckle sensor, due to intermittent modulation, measurement with the zero-crossing method requires some modifications. Typical mistakes with zero-crossing are shown in Fig. 4.6

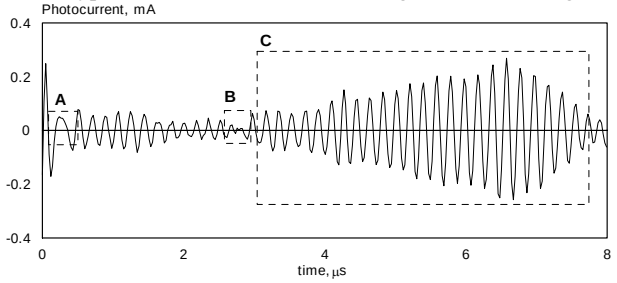

Figure 4.6. Typical mistakes with zero-crossing frequency measurements. Application of zero-crossing to part C of the signal will give a true result; application to parts B and A will give errors.

One can see in Fig. 4.6 that part C of the signal, which is referred to as information burst, contains almost equal periods of modulation. In contrast, part A will produce clearly erroneous results and should be considered a bad mistake. As for part B, measurement can hardly be accurately implemented using zero-crossing due to low SNR. Therefore, including the results of measurements obtained with parts A and B of the signal in the averaging procedure will only reduce the accuracy. However, simple logic, which can detect and eliminate evident mistakes before the averaging, can make the result much more accurate. So parts A and B of the signal will be not included in the averaging procedure.

In this study the zero-crossing technique was implemented not only by software simulation but also with a zero-crossing frequency meter. A frequency meter measures frequency in real time and transfers it to a PC, which processes the results and represents it as a text or graphics. The frequency meter consists of a comparator and a digital counter, and can be connected to the PC by means of a USB. The comparator generates short pulses when the input signal crosses the zero level. These short pulses are further transferred into the counter, which calculates the number of pulses, N_{SP}, within the counting window, Δt. The approximate length of the counting window is set by the operator. The length could be either 16 or 32 μs. The actual length of the window is defined as the time between the first and the last signal pulse occurring inside the approximate counting window. The actual length was measured by calculating the number of periods, M_{QP}, of the quartz generator operating at a frequency of 150 MHz. At the end of the counting window, the number of the signal pulses and number of the quartz periods are introduced into the computer using a FiFo circuit and USB port for further calculations. The next counting window starts immediately when the next signal pulse enters the calculator. In this way continuous measurement of the frequency of the photodiode signal was implemented. The frequency is calculated in the computer as

$$f_{SP} = \frac{N_{SP}}{M_{QP}} f_{QG}. \qquad (4.14)$$

Here f_{QG} is the frequency of the quartz generator. The first counting window starts synchronously with the beginning of the laser beam scanning. A single measurement could include a maximum of 512 counting windows. After the measurement is completed, the series of measured frequencies is acquired by the PC. Specially developed software can eliminate bad mistakes, implement averaging and recalculate the result into the z-distance by using Eq. 4.8 or Eq. 4.9. Finally the computer displays the measurement results, e.g. the

dependence of the measured z-distance on the current time, t_{SC}, which is readily re-calculated into the x-coordinate of the surface as $x = V_{LB} \cdot t_{SC}$.
The main disadvantage of the used zero-crossing frequency meter is the minimal counting window size of 16 μs. In the case of frequency of 10 MHz the minimal counting window includes about 160 periods of modulated photocurrent. Therefore, if the counting window contains at least one bad mistake (see Fig.4.6) then the result of measurement can be considered as a bad mistake also. This strongly decreases the performance of frequency meter. For more accurate measurements the smaller counting window size of 3-5 periods of modulated photocurrent is preferable. Therefore, zero-crossing frequency meter was used rather to demonstrate possibility to build the workable sensor prototype and most of the calculations and estimations were made using personal computer and saved photocurrent traces.

4.4 Arrangement of dynamic speckles distance sensor

On the basis of the principle explained above, one can easily produce a speckle distance sensor. The principle scheme is shown in Fig. 4.7(a). Here the laser beam expanded by a convex lens illuminates the moving surface. The surface is located behind the beam waist position (however, one can place it also between the lens and the beam waist position). The main condition to be satisfied is that the measurements should be made close to the beam waist position (but out of the Rayleigh range) where the largest gradient of frequency with distance change is observed, see Eq. 4.7 and Fig. 4.7(b). The scattered light is filtered with Ronchi rulings (Ronchi rulings are equal bar and space patterns with various periods) and collected into the photodiode. The frequency of the modulated photocurrent represents the distance to the object. The distance can easily be found using Eq. 4.7. A simple way to observe z-displacement of the object is to connect the photodiode to a digital oscilloscope and to apply FFT to the acquired signal. In this case the displacement of the FFT peak on the display of the oscilloscope represents the z-displacement of the surface of the object. Typical $f_{SP}(z)$ dependence on Eq. 4.7 is shown in Fig. 4.7(b).

The sensor needs some electronics to carry out the measurements and transfer data to the computer. The computer can process acquired data and represent the results as a profile picture on the display for the control or management of some industrial equipment of the working process in a feedback mode.

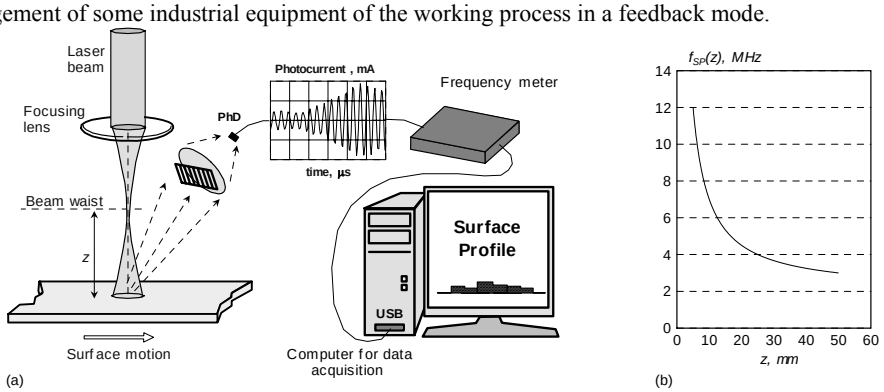

Figure 4.7. (a) Principle scheme of surface profile measurements by means of dynamic speckles and (b) the dependence of f_{SP} on z-distance for Eq. 4.7 (V_{OS} = *50 m/s,* D_o =*50 mm,* Λ =*50 μm*)

In spite of obvious simplicity of the sensor, to the best knowledge of the author no industrial sensor of this type has been built yet. The reason is discussed in next subsection.

4.5 Improvement of speckle distance sensor

There are two main disadvantages to the speckle sensor: (i) the short dynamic range of the dynamic speckle method, as a result of the limited scale range and high dispersion of measurements, and (ii) the dependence of the measurement procedure on the motion of the surface, which can be unstable or even discontinuous.

(i) Limited to several centimetres, the scale range of a SDS requires micron accuracy of a single *z*-coordinate measurement to provide an acceptable dynamic range. As was mentioned, measurement of the *z*-coordinate in a SDS is indirect but it is realized through measurement of the frequency of modulated light power after spatial filtering. The typical measurement procedure requires at least one period of modulation. For example, in the case of a pure sinusoid, one period of oscillation completely defines the frequency, since all periods of harmonic oscillations are equal. In the case of the speckle sensor, modulation of the photocurrent is stochastic and periods are not equal to each other. Estimation of the accuracy of the speckle method discussed in **paper IV** provides an accuracy of 110 μm after averaging over 50 periods of photocurrent oscillations. An accuracy of 110 μm does not provide the dynamic range suitable for most industrial application. It is clear that to increase the accuracy one has to average more periods of oscillations. According to the central limiting theorem, the deviation decreases as the square root of the ensemble length. Thus, averaging, for example, over 500,000 periods of oscillation will result in 1-μm accuracy, which already provides a much more reasonable dynamic range: for the 1 mm range it is 1,000:1 (μm).

However, to accumulate these 500,000 periods one requires a much longer measuring window. For the frequency of 100 kHz, the measuring window providing 1-μm accuracy is equal to 5 seconds. Such a long response time makes the sensor also not suitable for most industrial applications. Besides, in this case conventional touch sensors provide much better performance. However, there is a solution, which allows decrease response of the sensor - increasing the modulation frequency. For example, with a modulation frequency of 20 MHz required 500,000 periods are acquired within just 25 ms. This is equal to 40 measurements per second with 1 μm accuracy within a range of several centimetres. According to Eq. 4.9 the modulation frequency is inversely proportional to the period of a spatial filter and directly proportional to its position and object velocity. The period and position of a spatial filter cannot be chosen arbitrarily and, therefore, the modulation frequency is limited for any spatial filter, as it is shown in **paper III**. But object velocity is not limited. For the optimal location of a spatial filter (see **paper III**) the object velocity of ~1 m/s results in a frequency of ~100 kHz, see Eq. 5.7. To achieve a 20 MHz modulation frequency, an object moving with a velocity of ~200 m/s is required. This is too fast for most industrial processes.

(ii) As was mentioned in the previous paragraph, the accuracy and response time of the speckle sensor depend on the velocity of the object. It is assumed that this velocity is constant. If the velocity randomly varies in time, then accurate measurements become difficult or impracticable even with fast moving objects (if the velocity randomly varies with time, the measurement results will also vary in time even if the *z* is constant, see Eq. 4.7).

The above-mentioned features (i) and (ii) greatly reduce the area of application of the sensor, and moreover if the object is stopped, the sensor is idle.

Clearly, the speckle-distance measurement technique is very simple. However, it depends completely on object motion. Therefore, some innovations are needed to improve the speckle technique. In this thesis a novel approach to sensor development is taken, and a workable sensor with fast response time and high accuracy is presented.

The simplest ways to improve the sensor are:

- Fast scanning over the surface with a velocity higher than the typical object velocity. Fast scanning can be applied continuously to the same part of the object surface. This makes measurements completely independent of object motion, and measurements can be applied to static objects. Fast scanners are available on the market: acousto-optic deflectors (AOD), polygonal mirror scanners

(PMS), etc. The scanning velocity with modern scanners is hundreds of meters per second. This is much faster than an object velocity in typical industrial applications.

- Utilization of at least two spatial filters simultaneously makes it possible to make measurements independent of the object velocity (if it is not zero). In this case, there is a system of two equations 4.7, where each equation refers to one of the spatial filters used (Λ_1, D_1 and Λ_2, D_2). By solving this system, one can exclude velocity from the equations and represent the z-distance as a function of only two measured frequencies, as is demonstrated in **paper I**. This is also another approach for averaging: using several spatial filters simultaneously for measuring the frequency from several channels in parallel. In this case, a high dynamic range can be provided even for moderate velocities.

In the next section, development of scanning SDS is described. First it is demonstrated that velocity independence can be achieved by using two independent spatial filters (see **paper I)**. However, at the same time it is shown that in this case, the accuracy of the measurements decreases (the second spatial filter is not used for averaging). Furthermore, it is suggested that the accuracy can be increased by increasing the modulation frequency to average more modulation periods within the same measuring window. This can be done by fast scanning over a static or slowly moving object. By using a basic (homemade) double-face mirror scanner, it was demonstrated (see **paper III**) that the dynamic speckles created with scanning can be used in distance measurement. The same double-face mirror scanner revealed that the modulation frequency is limited by geometrical parameters (such as Λ, D_o etc.) and can be increased only by using a faster scanner. Thus, to improve SDS performance, more advanced scanners were required, and an acousto-optic deflector (AOD) was chosen (see **paper II**). It was shown that in the case of an AOD and diffraction from a variable acoustic wave, the generated dynamic speckles are also suitable for distance measurement. Using an AOD at scanning velocities of 50-150 m/s it was shown that an accuracy of 110 μm can be achieved within just 2.5 μs (see **paper IV**). For further improvement of the sensor parameters, a faster AOD was used (see **paper V**) and its performance was compared with that of the slower one. The properties of polygonal mirror scanners are discussed at the end of the section, because a polygonal mirror scanner obtains the same order of scanning velocity and can be an alternative to an AOD scanner.

5 A scanning dynamic speckle sensor

5.1 Velocity independent measurements

This subsection describes how the idea of using a fast scanner arose from consideration of a velocity-independent measurements scheme. It also demonstrates the possibility of using several spatial filters simultaneously for averaging. Consideration of Eq. 4.7 suggests a simple way to make distance measurements velocity independent: by installing two different Ronchi rulings with spatial periods of Λ_1 and Λ_2 at different distances D_1 and D_2 from the focal point. Thus, the power of the transmitted light will be modulated at the frequencies of f_{SP1} and f_{SP2}, respectively, according to Eq. 4.7:

$$f_{SP1} = \frac{V_{OS}}{\Lambda_1}\left(2 + \frac{D_1}{z}\right), \quad f_{SP2} = \frac{V_{OS}}{\Lambda_2}\left(2 + \frac{D_2}{z}\right). \qquad (5.1)$$

After simultaneous measurement of the modulation frequencies f_{SP1} and f_{SP2}, the distance z between the focal point and the moving surface is calculated as in **paper II:**

$$z = \frac{D_2\Lambda_1 f_{SP1} - D_1\Lambda_2 f_{SP2}}{2(f_{SP1}\Lambda_1 - f_{SP2}\Lambda_2)} \qquad (5.2)$$

Here D_i and Λ_i, are completely defined by the sensor geometry and can be precisely calibrated. Therefore, by measuring f_{SP1} and f_{SP2} the absolute distance to the surface can be determined. To test the technique, the setup schematically shown in Fig. 5.1 was used.

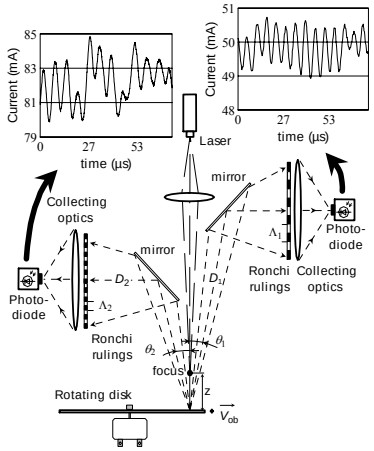

Figure 5.1. Setup for distance measurements using spatial filtering of dynamic speckles. Inserted charts show typical oscilloscope traces of electrical current recorded from both photodiodes simultaneously.

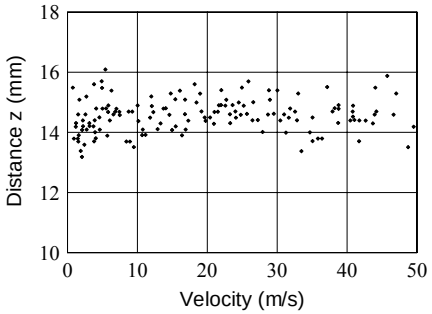

Figure 5.2. Distance z as a function of the surface velocity V_{OS} calculated from Eq. 5.2. Modulation frequency f_{SP1} and f_{SP2} of the spatially filtered speckle patterns was measured using fast Fourier transforms of photodiode signals.

The results of the measurements are shown in Fig. 5.2, where the calculated value of z is plotted as a function of the surface velocity. As can be seen, it is independent from V_{OS} in the wide range of velocities. The average value of z = 14.6 mm coincides with z = 15.0 ± 0.5 mm measured by the conventional technique.
The root-mean-square error of the z-measurements shown in Fig. 5.2 is Δz = 0.7 mm, resulting in the relative measurement inaccuracy of $\varepsilon_z = \Delta z/z = 0.048$, which is in accordance with the theoretical estimation given by the next equation:

$$\varepsilon_z = \frac{(2z + D_1)\cdot(2z + D_2)}{\sqrt{2}\cdot z|D_1 - D_2|}\varepsilon_f , \qquad (5.3)$$

here ε_f is the relative inaccuracy of the frequency measurements.

The accuracy of the z-coordinate can be improved at the expense of x-coordinate resolution by acquiring a longer modulated photocurrent. However, the inaccuracy in the case of two filters and unknown object velocity is worse in comparison with a single spatial filter and known object velocity. With a single filter and known constant surface velocity, the relative inaccuracy is given by the next equation:

$$\varepsilon_{z_o} = \frac{(2z + D_1)}{D_1}\varepsilon_f \qquad (5.4)$$

From Eq. 5.3 and Eq. 5.4 it can be seen that if ε_f is constant then ε_z is larger in the case of unknown velocity measurements by means of two spatial filters, due to the greater multiplier factor of ε_f:

$$\frac{\varepsilon_z}{\varepsilon_{z_o}} = \frac{D_1}{\sqrt{2}\cdot z}\frac{(2z + D_2)}{|D_1 - D_2|} \qquad (5.5)$$

Using reasonable filters positions of 20-150 mm and a z-coordinate of 1-10 mm, the ratio $\varepsilon_z / \varepsilon_{zo}$ is always greater than one. Therefore, the accuracy of measurements with two spatial filters when the object velocity is unknown is worse than in the case of one spatial filter and known object velocity.

Simple realization of spatial filtering suggests utilizing an array of filters for data averaging. In this case, if object velocity is known and each spatial filter is independent, then simple averaging of two channels will improve accuracy whatever is the position of each filter. The use of more than two spatial filters can make measurements velocity independent and more accurate, due to averaging over many channels.

The other approach to making measurements independent of object velocity is scanning over the object surface. This solution is preferable since, in contrast with two filters, it works even with static objects. Using an acousto-optic deflector or polygonal mirror scanner, the scanning velocity can achieve hundreds of meters per second and measurements can be independent of slow object motion.

5.2 Review of various scanning techniques

Light beam deflection techniques are well-developed and are utilized in a number of commercially available products such as printers, scanners, IR imagers, optical inspection machines, bar-code readers, etc. The most commonly used beam deflectors are polygonal mirror scanners, holographic scanners and acousto-optic beam deflectors (AOD) [42]. Although the operational principle of holographic scanners is different from that of the rotating mirror, holographic scanners provide a generic equivalent of the rotating mirror. Ultimately the scanning velocity of both is defined by the rotation speed of the electrical motor used, and limited by several hundreds of meters per second. In contrast, there are no mechanically moving parts in an AOD [43,44] and it can provide even higher velocities of the deflected beam (up to 1,000 m/s). The operational principle of the AOD is light diffraction from the acoustic wave running inside an acousto-optic crystal. Frequency modulation of the excited acoustic wave leads to a change in its wavelength and so to a change in the diffraction angle, thus providing deflection of the readout beam. The scanning velocity achievable in an AOD is determined by the parameters of the acousto-optic crystal and by the optics and electronics used.

In this thesis, polygonal and acousto-optic scanners are considered. The principle of an AOD and a PMS, and the parameters of the deflectors utilized, are given in appendix A. Both scanners possess the same order of scanning velocity, which is within 500 m/s. Both scanners were studied experimentally and the results are presented below. In the next subsection a basic polygonal scanning profilometer, which uses a double-face mirror, is described.

5.3 Double-face mirror profilometer

5.3.1 Operation of mirror profilometer

The operational principle of a polygonal mirror SDS is as follows: the expanded laser beam is deflected with a PMS and thus it scans over the object surface; the light scattered from the surface is optically filtered by Ronchi rulings and then collected into a photodiode; the temporal frequency of the photodiode current is continuously measured with a zero-crossing frequency meter and it is further recalculated into the distance z using Eq. 4.9. In this work a simple double-face mirror located on the axis of an electrical motor was used. A block-diagram of the experimental set-up is shown in Fig. 5.3. For more details see **paper III**.

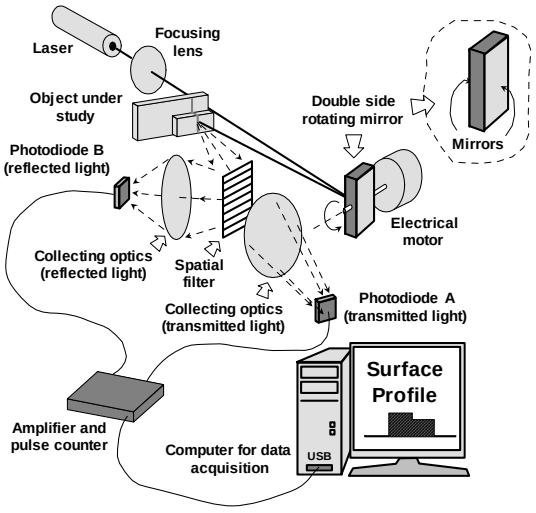

Figure 5.3. Dynamic-speckle profilometer. A dynamic speckle pattern is generated by the laser beam scanning the surface under study. Scanning is accomplished by means of deflecting the laser beam from the rotating double-face mirror fixed on the axis of the electrical motor. To improve SNR, the power of the reflected light was used together with the transmitted light.

To demonstrate the feasibility of the proposed technique for surface profile measurements, a metallic plate with a 1 mm step was used as the test object. A photograph of the plate is shown in the inset of Fig. 5.4(a). In this experiment, the laser beam scans the object surface with a velocity of V_{LB} = 12 m/s. The plate was situated so that the distance from the illuminating beam waist to the upper level is 3 mm.

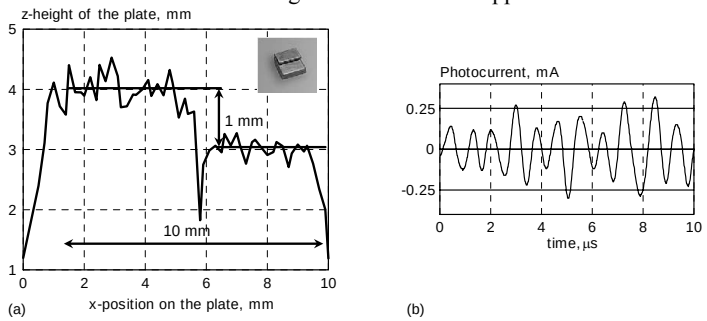

Figure 5.4. (a) Profile measurements of the aluminium plate with 1 mm surface step using a dynamic-speckle profilometer with scanning implemented by a rotating mirror. Photograph of the plate is shown in the upper right corner, (b) A typical photocurrent

A typical experimental 2D-scan of the plate is shown in Fig. 5.4(a). Each scan was accomplished within the time window of 800 μs. The upper level measurements include 28 counts of the zero-crossing frequency meter resulting in $z_1 = (4.0 \pm 0.3)$ mm while there are 20 counts for the lower level with $z_2 = (3.0 \pm 0.2)$ mm. The modulation frequency at the upper level is 0.8 MHz and 0.6 MHz at the lower level. A typical trace of the photocurrent is shown in Fig. 5.4(b). The measurement accuracy for both levels was calculated as the root-mean-square deviation from the averaged value. Therefore, the measured step is (1.0 ± 0.3) mm and it is in accordance with the measurements accomplished by the conventional method (by means of the vernier caliper with a resolution of 0.03 mm).
The resolution of the technique along the direction of scanning is defined by the laser spot at the surface and/or by the displacement of the spot during the measuring window Δt, depending on which of these two values is larger. In this particular experiment the illuminating spot displacement was 200 microns and its diameter on the lower step (which is situated farther from the beam waist then the upper level) was 320 microns. The latter value can be considered as the resolution along the scanning direction in this particular implementation of the profilometer.

Detailed analysis of the measured profile shows that the main reason for the inaccuracy in z-measurements is erroneous calculation of the number of zero-crossing points using the frequency meter. In this particular implementation of the profilometer the program managing the zero-crossing meter did not detect the bad mistakes. Therefore, for example, Fig.5.4(a) contains the noticeable downward excursion in the middle of the chart as the signal from the respective step on surface possesd low SNR. The accuracy can be improved by decreasing the counting window and including the algorithm of detecting and eliminating bad mistakes into the electronics. In its turn, the response time can be easily decreased by increasing the modulation frequency. The modulation frequency depends on the geometry (see Eq. 4.9) and on the scanning velocity. Further research revealed that the modulation frequency can be increased only with faster scanning.

5.3.2 Limits of the spatial filtering technique

To optimize the profilometer and find the limits of its performance, the experimental geometry was changed. The aim was to increase the modulation frequency with the given object velocity by varying the period and

location of the spatial filter. The dynamic speckles in this experiment were generated with a disk rotating at a constant angular speed illuminated with a static laser beam. The disk was mounted on the translation stage allowing precise positioning of the surface in the range of 0-50 mm. The spatial filter was also mounted on another translation stage. Five different Ronchi rulings with spacing Λ of 25.4 μm, 42.5 μm, 64.5 μm, 125 μm, and 254 μm were sequentially tested for spatial filtering of the scattered light. The photodiode current was stored by digital oscilloscope and FFT was applied to estimate the SNR, and the modulation frequency, f_{SP}. The rotating disk had a flat surface so the distance from the beam waist to the disk surface was constant. An invariable distance to the surface provides constant frequency of the spatially filtered light power modulation. SNR measurements were carried out in a wide range of D_o and z variations.

Figure 5.5 shows the position of the surface as a function of the spatial-filter position for the condition of SNR = 5 dB measured for spatial filters with different spacing, Λ.

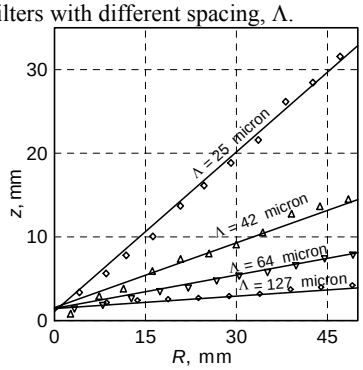

Figure 5.5. Pairs of filter positions and distances to the surface at which SNR = 5 dB (estimated using FFT) for spatial filters with different spatial periods. The area above each line corresponds to the geometry when the signal is modulated at a well-defined frequency, while in the area below the modulation is irregular.

One can see that the dependence $z(D_o)$ is linear. The area above each line in Fig. 5.5 defines the combination of z and D_o where regular modulation of the light power can be confidently measured, while below the line regular modulation is not observable. To explain this, it should be pointed out that the average diameter of the speckles (see Eq. 4.3) depends on the distance between the illuminated area and the position of the spatial filter, as follows:

$$d_{SP} = 2r_S = \frac{2 \cdot \lambda}{\pi \cdot NA}\left(1 + \frac{D_o}{z}\right). \qquad (5.6)$$

Therefore, locating the spatial filter at a larger distance D_o or approaching the tested surface to the beam waist will lead to increasing the average speckle size. The linear dependence $z(R)$ shown in Fig. 5.5 means that the signal always disappears when the average speckle size reaches a certain value. This boundary value (see **paper III)** was found to be equal to the spatial period, Λ, of the spatial filter used. By comparing Eq. 4.9 with Eq. 5.6 it can be deduced that the modulation frequency and average speckle size have a similar dependence on z and D_o. The equation for the highest achievable frequency of the light modulation can be readily derived from equations 4.9 and 5.6, introducing the condition of $d_{SP} = \Lambda$:

$$f_{SP}^{\max} = V_{LB}\frac{\pi \cdot NA}{2 \cdot \lambda} \qquad (5.7)$$

It can be seen that the modulation frequency for a given spatial filter is limited by $f_{SP}^{\max}$. Moreover, the highest achievable frequency is independent of the filter position, its spacing and distance to the surface. In

accordance with Eq. 5.7, $f_{SP}^{\max}$ is directly proportional to the scanning velocity, V_{LB}, and it depends on the numerical aperture of the illuminating beam and the light wavelength. This was experimentally proved for different NA and Λ.

Therefore, a double-faced mirror SDS, a detailed analysis of which is given in **paper III**, demonstrated that it is impossible to obtain regular modulation with any spatial filter if the spatial period Λ is smaller than the average speckle size. The boundary condition $d_{SP} = \Lambda$ is true in all geometries of the experiments for all the filters used. Since NA is limited, there is an absolute maximum of the modulation frequency that can be theoretically achieved for a given scanning velocity and light wavelength when the spatial filtering technique is used for speckle velocity measurements. However, fast continuous scanning over the object surface many times can improve the accuracy by the factor $\sqrt{N}$, where N is the number of scans (it is assumed that scans are statistically independent). The disadvantage of multiple scanning is the longer response time of the sensor. Therefore, it is preferable to use a faster scanner rather than a homemade double-face rotating mirror. The fast reliable scanner can be realized by using an AOD.

5.4 A scanning speckle sensor based on an acousto-optic deflector

The first experiment was accomplished using an AOD based on a TeO_2 crystal and it is presented in **paper II**. A piezoelectric transducer generated transverse acoustic waves propagating along the [110] crystal axis with a velocity of V_{AC} = 690 m/s. The scheme of measurements is the same of that of the polygonal SDS. The only difference was that the beam was deflected with an AOD. The main result of the experiment with the AOD was to demonstrate the possibility of getting pronounced modulation with a laser beam deflected by an acousto-optic crystal. The wavelength of the laser beam deflected by the AOD is a function of the deflection angle due to the Doppler shift acquired by the beam when it diffracts from the running acoustic wave. This leads to variable phase shift of the illuminating beam during the scan and may affect the formation of the dynamic speckle pattern. However, our experiments showed that such an influence is insignificant, so the spatial filtering technique of dynamic speckles can be used for distance measurements.

In the series of experiments it was demonstrated that an AOD sensor is capable recognizing the same plate profile as was done with the polygonal SDS (see Fig. 5.4). A typical measurement of the profile is shown in Fig. 5.6. It is worth noting that length of the scan at the object surface in case of the AOD was smaller (5 mm) than in case of double-face rotating mirror scanner (10 mm). Therefore, only the central part of the test object near the step on the surface was scanned.

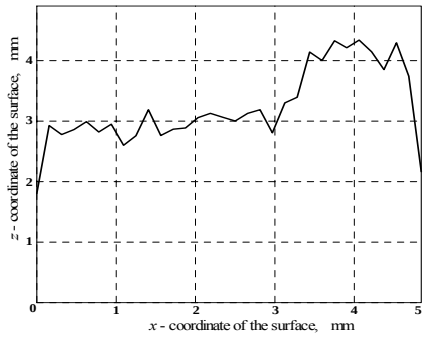

Figure 5.6. Profile measurements of the aluminium plate with 1 mm surface step using an AOD sensor with scanning implemented by an AOD. A photograph of the object (plate) is shown in Fig. 5.4.

A scanning velocity of 10 m/s leads to the modulation frequency of the spatially filtered light varying in the range of 100 – 500 kHz depending on the *z*-position of the surface. The scanning velocity is naturally defined by the total scanning time provided by the acousto-optic deflector. The minimal time supported by the AOD is the travel time of the acoustic wave through the aperture of the AOD. For the particular deflector used in the experiment, the travel time is 13 μs. According to Eq. 4.9 the modulation frequency is directly proportional to the scanning velocity. However, the experiments showed that the function $f_{SP}(V_{LB})$ remains linear only up to 40 m/s (respective scanning time of 100 μs). Thereafter, the modulation frequency is saturated even though the modulation is well pronounced. The reason for the frequency saturation is discussed in **paper IV**.

The experiment was successful; however, it was not carried out in optimal conditions, according to the findings of **paper III**. The highest modulation frequency is achieved when the speckle size is equal to half of the filter period, as was discussed in the previous section. In this case the maximal frequency is proportional to the scanning velocity and independent of the filter position and its period. The experiment with the double-face mirror sensor was made in optimal geometrical conditions and the frequency of 2 MHz was achieved with a scanning velocity of 16 m/s. As the scanning velocity with an AOD was of 130 m/s, a modulation frequency of 16 MHz was expected. However, only 6 MHz was achieved. This is believed to be a consequence of the non-optimal geometry of the experiment. Optimization of the geometry was made in the experiment described in **paper IV,** where the phenomenon of frequency saturation with growth in the scanning velocity is also analyzed.

5.5 Estimation of AOD sensor performance

5.5.1 An AOD sensor in an optimal geometry

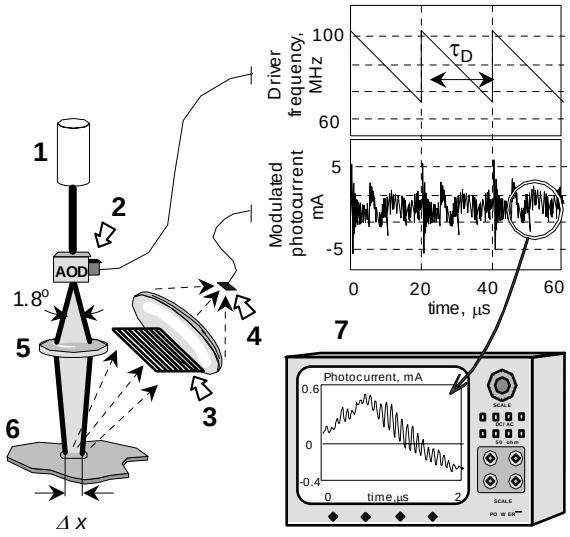

Figure 5.7. Optical set-up of the distance sensor based on spatial filtering of dynamic speckles generated via acousto-optic deflection of the laser beam over an optically rough object surface. 1 - Laser, 2 - AOD driver, 3 - Spatial filter and collecting optics, 4 - Photodiode, 5 - Focusing optics, 6 - Object surface, 7 - Digital oscilloscope.

The experiment with the AOD described in the previous section was not optimized in terms of the position of the spatial filter. As was demonstrated by the example of the double-face mirror profilometer, the average speckle diameter should be equal to the half-period of the spatial filter (see **paper III**). In this case, the

modulation frequency is maximal. In this section the experiment with the AOD is optimized and sensor performance in optimal conditions is estimated. The layout of the setup for the experimental study of the proposed distance sensor is shown in Fig. 5.7 and a detailed description of the experiment is given in **paper IV**. The photocurrent was measured by a digital oscilloscope. Due to the optimal sensor geometry and scanning velocity of 100-150 m/s, a modulation frequency of 15-20 MHz was expected.

A typical oscilloscope trace of the photocurrent recorded in optimal geometry is shown in Fig. 5.8. As can be seen, the shape of the light power modulation is much close to the sinusoidal.

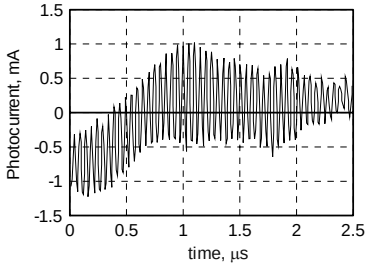

Figure 5.8. Typical oscilloscope traces of the photocurrent recorded at a scanning time of 20 μs (a).

The maximal modulation frequency observed in the experiment with the optimal sensor geometry was 35MHz, which was 2 times higher than expected (15-20 MHz). This is explained by the higher output power of the Nd:YVO_4 laser compared with the He-Ne used in previous experiments. Higher output power of the laser increases the number of photons collected to the photodiode and results in higher SNR, as is reported in **paper V**. The experiment proves that the modulation frequency is defined mainly by the scanning velocity. Since the output power of the laser is limited, the geometry of the sensor is optimized, and the numerical aperture of the illuminating beam cannot be greater than unity, increasing the scanning velocity is the main approach to improve the sensor. The dependence of the modulation frequency on the *z*-distance is shown in Fig. 5.9.

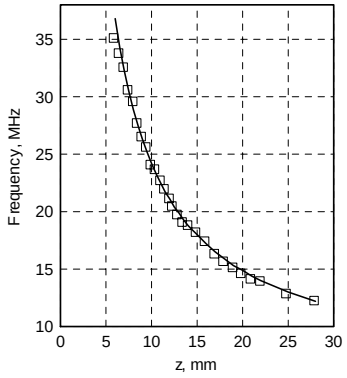

Figure 5.9. Modulation frequency of the light power of the spatially filtered speckle pattern as a function of the *z*-distance between the object surface and the illuminating beam waist. The squares are the experimental points and the solid line is the theoretical curve of Eq. 4.9.

An AOD provides a fast scanning velocity. However, the scanning velocity of an AOD is limited by the travelling time of the acoustic wave within the aperture of the acousto-optic crystal (or through the beam diameter if the latter is smaller then the active crystal aperture). Note that the travelling time of the acoustic

wave through the crystal aperture is 13 μs, which is a bit smaller than the scanning period of 20 μs for the trace in Fig. 5.8. In this case, different parts of the light beam diffract from the acoustic wave at different angles because the wave frequency varies faster than the wave propagates through the beam, as is demonstrated in **paper IV**. This is a well-known effect of the dynamic defocusing of the light beam in an AOD at fast rates of deflection [45].

When the scanning time approaches the travelling time, saturation of the modulation frequency takes place. The dependence $f_{SP}^{\max}\left(\tau_D^{-1}\right)$ has been measured for different diameters of the laser beam incident into the AOD. This dependence was expected to be linear according to Eq. 4.9. However, it was found that deviation from the expected linear growth of the modulation frequency becomes pronounced when the light beam diffracts from an acoustic wave whose frequency is swept along the light beam diameter. As can be seen in Fig. 5.10, the wider the variation of the acoustic wave frequency within the light beam, the larger the observed deviation from the initial linear dependence. These experiments show that the increase in the modulation frequency (which is the key parameter for improving the accuracy and response time of the sensor) is limited by the travelling time of the acoustic wave. By using a deflector operating with acoustic waves of higher velocity, a higher modulation frequency can be achieved.

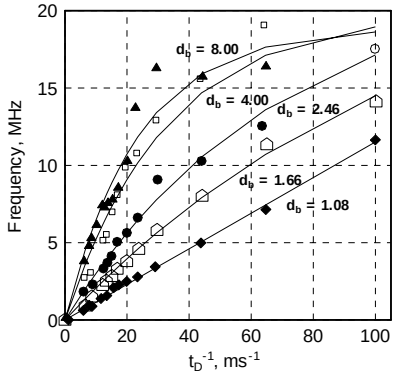

Figure 5.10. Dependence of the highest achievable modulation frequency on the inverse time duration of the beam scan.

5.5.2 Accuracy estimation

The accuracy of *z*-coordinate measurement estimation was reported in **paper IV**. The accuracy is completely defined by the accuracy of the frequency measurements. Photocurrent oscillations excited by spatially filtered dynamic speckles are not constantly regular. In this case, the simplest way to improve accuracy is accumulating and averaging the results of measurements. Data accumulation increases the response time of the sensor, creating a trade-off between accuracy and response. To estimate this trade-off, the scanning beam of the maximal diameter, which is equal to the optical aperture of the AOD, according to **paper IV**, was used.

Experimentally the trade-off between *z*-accuracy and response time was estimated using a plain metal plate located at the distance z_0 = 11.5 mm from the focal plane of the illuminating beam. The flatness of the plate surface was checked with a conventional contact profiler and was within 2 μm. The sample was held in a precise computer-controlled support which allowed plate displacement in three orthogonal directions with an inaccuracy of less than 0.5 μm. The support was oriented so that one of the directions of displacement coincides with *z*. One hundred statistically independent measurements of the *z*-distance were carried out. The AOD deflector was oriented to scan the sample surface in the *x*-direction with the scanning time τ_D = 20 μs. After each measurement, the sample was randomly displaced along the y-axis, keeping the position z_0 equal to 11.5 mm. During the scan the photodiode signal was recorded within the time window of 2.5 μs, which

includes approximately 50-55 periods of oscillations. In this experiment the modulation frequency f_{SP} was estimated by measuring each oscillation period of the recorded signal by means of peak detection, and then averaging the data within the time window. The distance to the plate surface was calculated using Eq. 4.9. The measured distance is dispersed around the mean value $\bar{z}$ = 11.50 mm, which coincides with z_o = 11.50 mm. The standard deviation from the mean value is 110 μm. Both the mean value and standard deviation were estimated for the ensemble of 100 measurements. The dispersion of the measured *z*-coordinate is shown on Fig. 5.11. The square points in Fig. 5.11 show experimental estimation of the *z*-distance probability density function, which was calculated from experimental data. The solid line in Fig. 5.11 is the Gaussian probability density function, which fits well the experimental data if the standard deviation is equal to 110 μm. According to the central limiting theorem, the deviation decreases as the square root of the ensemble length. Therefore, by collecting the data after multiple scanning of the surface and/or measuring frequency with several spatial filters simultaneously, sensor accuracy can be improved.

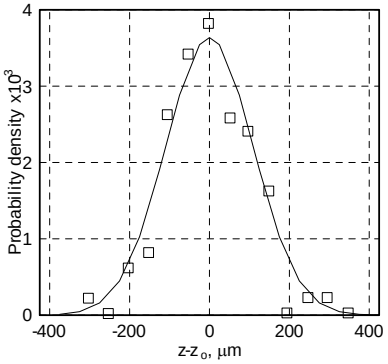

Figure 5.11. Dispersion of the measured *z*-distance around the fixed position z_0 in the set of 100 measurements, each of which was done during 2.5 μs.

These experiments demonstrate that the regime of acousto-optic deflection from the wave of variable frequency is still applicable for distance measurements using dynamic speckles, but it creates limitations for the improvement of the response time and accuracy. According to the data shown in Fig. 5.10, it is the velocity of the acoustic wave that finally defines the maximal achievable modulation frequency. The higher velocity of the acoustic wave, the smaller the travelling time achieved for the same aperture of the light beam. In the particular AOD used in the experiments, the velocity of the acoustic wave was 690 m/s. Using the same TeO_2 crystal but in a different geometry, the wave velocity can be increased up to 4200 m/s. By using such a fast AOD it is expected that the modulation frequency can be increased by an order of value and thus reduce the response time. A comparison of two AODs with different acoustic wave velocities is given in **paper V**.

5.6 Comparison of acousto-optic deflectors

In this section two AODs with different acoustic-wave speed are compared. The detailed comparison of two deflectors is reported in **paper V**. The first deflector, named "slow", with an acoustic wave velocity of 690 m/s is the one which was used in the experiment described in the previous sections. In comparison with the slow deflector, the second, named "fast", possesses a higher acoustic wave velocity. The fast AOD was made of the same acousto-optic crystal TeO_2 as the slow one but the transducer generates a longitudinal acoustic wave along the [001] axis. The acoustic wave velocity for the fast AOD is $V_{[001]}$ = 4200 m/s, which is six times larger than for the slow AOD, $V_{[110]}$ = 690 m/s.

The parameters of both deflectors are listed in Table A1, see appendix A. The main difference between the slow and fast deflectors are the diffraction efficiency and the size of the active aperture. The slow AOD has

uniform diffraction efficiency at the level of 80 % along the whole optical aperture. In contrast, the diffraction efficiency of the fast AOD is non-uniform and rapidly attenuating along the optical aperture. The relative area of the active optical aperture in the fast AOD is at least 100 times smaller than that of the slow AOD. Moreover, the active aperture of the fast AOD is stretched along the acoustic-wave propagation direction.

The active optical aperture of the crystal defines the numerical aperture of the illuminating beam, and the latter defines the maximal modulation frequency in Eq. 5.7. The diffraction efficiency of the AOD is also an important parameter for the SDS. The number of photons collected to the photodiode defines the SNR of the electric signal. Experiments described in **paper V** demonstrate an increase in the modulation frequency with an increase in the light power of the laser. This phenomenon can be explained by the fact that SNR increases at high laser power, thus allowing a closer approach to the focal plane of the focusing lens. Smaller z results in higher frequency, in accordance with Eq. 4.9.

Light power collected to the photodiode is a more critical issue for the fast AOD because its diffraction efficiency is an order of value smaller. Moreover, the rectangular shape of the acoustic channel of the fast deflector requires the use of cylindrical optics to transform the incident laser beam from a circular cross-section to a truncated rectangular beam. Cylindrical optics allows a notable increase in the diffraction efficiency. However, the diffracted light power for the fast AOD is still 10 times less than for the slow one. Therefore, in the case of the 1-W-laser (which was used in the experiment), the maximal frequency for a slow AOD can be expected to be about 2 times smaller than for the fast one, as was shown in **paper V**. In Fig. 5.12 the dependence of the modulation frequency on z-coordinate is shown, see Eq. 4.9. It can clearly be seen that the maximal frequency in the case of the fast AOD is 2.3 times higher. This is well in accordance with the shorter footprint (defined by angular band, see appendix A) and smaller diffraction efficiency of the fast AOD.

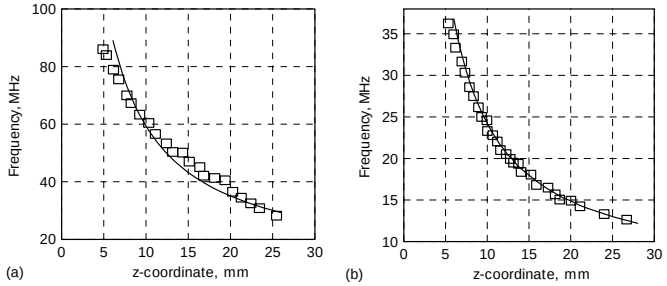

Figure 5.12. Modulation frequency of the light power of the spatially filtered speckle pattern as a function of the z-distance between the object surface and the illuminating beam waist. The squares are the experimental points and the solid line is the theoretical curve of Eq. 4.9: (a) fast deflector and (b) slow deflector.

The fast AOD demonstrates the same frequency saturation as the slow one. As was expected, the frequency saturation for the fast AOD is achieved later because the acoustic wave velocity is greater and, consequently, the travelling time through the crystal aperture is shorter.

Fig. 5.13 shows typical oscilloscope traces for slow and fast deflectors. In spite of the fact that the modulation frequency with a fast deflector is higher and the response time is shorter, the filling up of the scan with informative modulation is smaller. In the case of the fast deflector, only 15-20% of the scan is filled with well-defined modulation, while the other part of the scan is just noise. In the case of the slow deflector, the

informative modulation is more pronounced and it takes almost 50% of the scan. After averaging data of many scans, the same number of oscillations per averaging time will be obtained with both deflectors.

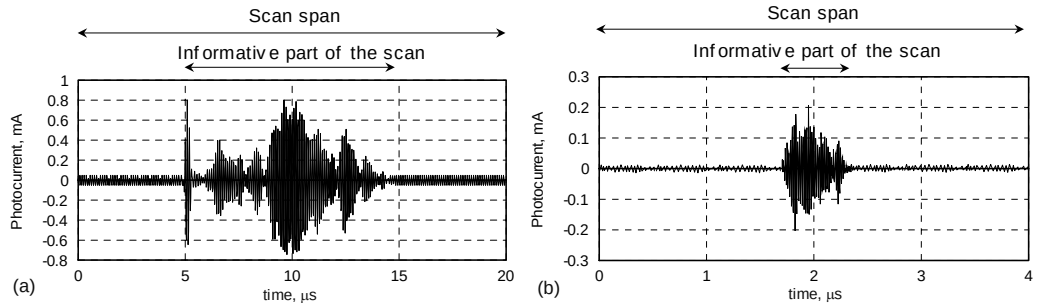

Figure 5.13. Typical oscilloscope traces. Only informative parts of the scans containing well-defined modulation are presented here: (a) slow deflector, central frequency f_{CI} ~ 10.5 MHz, scan duration τ_D = 20 μs, informative part duration ~ 10 μs, (b) fast deflectors, central frequency f_{CI} ~ 65 MHz, scan duration τ_D = 4 μs, informative part duration ~ 0.6 μs. Both traces are filtered with band frequency filters with cut-off frequency of $f_{CF} = f_C \pm 0.2 f_C$.

Comparison of two acousto-optic deflectors for scanning implementation in the dynamic-speckle distance-measurement application showed that the most important deflector parameters which affect the performance of the proposed sensor are

- the acoustic wave velocity in the crystal
- the active aperture of the acousto-optic crystal
- the diffraction efficiency
- the angular band

A higher modulation frequency was achieved with the fast deflector than with the slow one. However, the maximal frequency of 80 MHz with the fast deflector is only 2.3 times higher than that of the slow deflector, 35 MHz, whereas an increase proportional to the acoustic velocity ratio $V_{[001]}$ / $V_{[110]}$, i.e. 6 times, was expected. The main reason of smaller frequency with the fast deflector than expected is the much smaller diffraction efficiency of the fast AOD, which reduces SNR of the modulated light power. In addition, the fast AOD has a smaller active aperture and smaller angular band, which also diminished the maximal achievable frequency.

In spite of the smaller than expected modulation frequency, the experiments clearly proved that the response time of the technique is defined by acoustic wave velocity. However, the speckle-distance measurements require averaging over several scans to increase the accuracy of the measurements. In the case of the fast deflector, only 15-20% of the scan is filled with informative modulation, while in the case of the slow deflector it is 50%. Thus, after averaging the number of oscillations, obtained with the fast scanner is almost the same as with slow one for the fixed time window and it does not give any important benefit.

5.7 Polygonal mirror scanner

In section 5.3 an alternative to an acousto-optic deflector double-face mirror scanner was presented. The mirror was taken from a laser jet printer and contained only two facets. The mirror was set into motion by a conventional electrical motor with a maximal achievable rotation speed of 15,000 rpm. The declared rotation speed was limited to 5,000 rpm, and rotation at faster angular velocities was accompanied by noticeable vibrations. The scanning velocity corresponding to the rotation speed of 15.000 rpm was limited to 50-70 m/s. However, the use of zero-crossing frequency meter for profile recognition (see section 5.3.1) was possible only for scanning velocities within 20 m/s (5000 rpm). At faster scanning speed (> 5000 rpm), owing

to the vibrations, SNR in acquired photocurrent was low and for the 15000 rpm angular speed the zero-crossing frequency meter could not resolve even the 1 mm step of the aluminium plate.

Vibrations and low scanning velocity prevent the use of homemade double-face mirror scanners in a SDS. However, polygonal mirror scanners are well-developed and available on the market. The operation of such scanners is not subject to vibrations, and the rotation speed achieves 50,000 rpm and even higher. The mirrors utilized in the PMS can have up to 72 facets, which is an important parameter for scan size optimization. The principle scheme of the polygonal scanner, basic equations and explanations concerning its operation are given in appendix A.

In this section a SDS using a fast polygonal scanner is presented. The scheme of a SDS based on a PMS is shown in Fig. 5.14. Here the number of mirror facets was 8 and the maximal rotation speed of the electrical motor was 30,000 rpm.

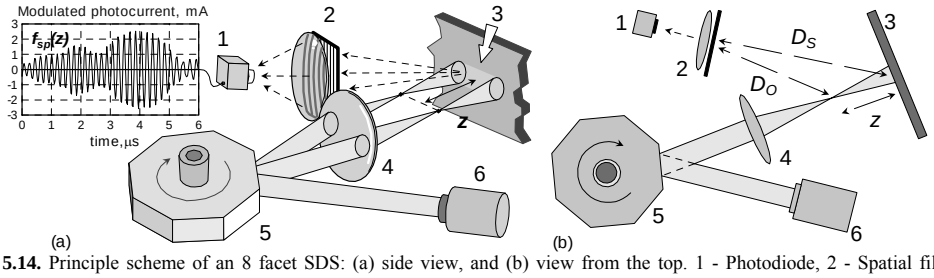

Figure 5.14. Principle scheme of an 8 facet SDS: (a) side view, and (b) view from the top. 1 - Photodiode, 2 - Spatial filter and Collecting Lens, 3 - Object Surface, 4 - Focusing Lens, 5 - Scanner, 6 - Laser.

The SDS scheme shown in Fig. 5.14 allows a modulation frequency of 10-15 MHz to be achieved. A typical photocurrent trace using the suggested scheme is shown in Fig. 5.15. It can be seen that the modulation is well-pronounced and the frequency can be easily estimated using even the zero-crossing method.

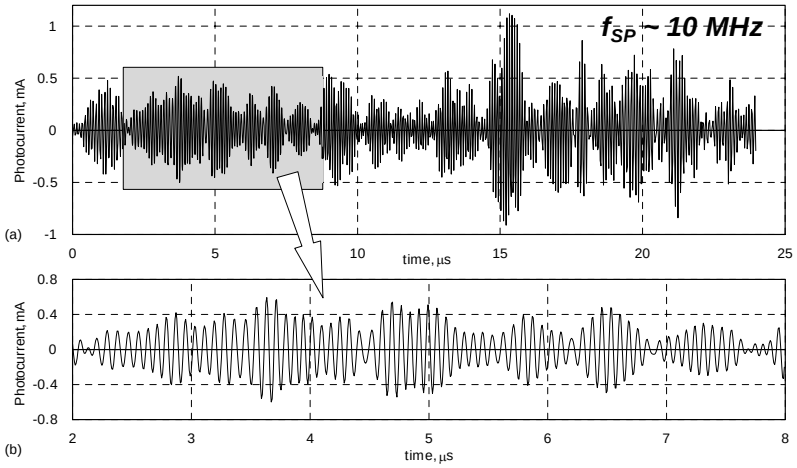

Figure 5.15. Typical oscilloscope trace obtained with a polygonal mirror scanner. Modulation frequency is ~10 MHz. The upper chart (a) represents 0-25 μs part of the scan, and the lower chart (b) represents 2-8 μs part of the scan.

The length of the informative component with an 8-facet PMS was 30-80 μs, which is much longer than with an AOD at the fastest regime. However, in the case of the AOD, 50% of scan contained well-defined modulation, whereas in the case of the 8-facet polygonal scanner the ratio of the informative modulation to scan duration was only 15-30%. This was defined by the entire scan duration of 250 μs for the 30,000 rpm angular speed and small number of facets. However, this ratio can be improved for a mirror with more then 8 facets. It is expected that the informative component ratio in acquired modulation can achieve 80% using a 72-facet mirror. The high informative component ratio together with the modulation frequency of 30 MHz achievable with a faster electrical motor equalizes the performance of a sensor based on a PMS and one using an AOD.

In this section detailed analysis of scanning was introduced. Fast scanning is quite easy to implement using either an AOD or a PMS. Both scanners result in a high modulation frequency of tens of megahertz and a corresponding short response time of a hundred nanoseconds. This allows the accuracy to be increased by means of averaging over time using information about the z-distance accumulated from many scans. Averaging brings up the question of a statistically independent sample. The basic example of a statistically dependent sample appears when the sensor repeatedly scans the same part of the object surface. In this case the photocurrent shape is constantly the same and averaging does not work. This is a very important issue for the optimal operation of a SDS. This issue is investigated in the next section.

6 Statistical properties of spatially filtered dynamic speckles

6.1 Importance of correlation

The statistical properties of dynamic speckles have attracted the attention of many research groups since the 1960s [46,47], when it was recognized that changes in the speckle pattern are somehow related to the object's motion. The search for deep understanding of dynamic-speckle behaviour was stimulated by a number of promising applications. The typical configuration considered in most previous works dealing with dynamic speckles involves an object moving in respect to the rest laser beam and the rest observer (concerning both velocity [48,49] and *z*-distance [4] measurements). Scanning the object with a laser beam and subsequent spatial filtering of dynamic speckles, reported in **papers II and III,** also exploits dynamic speckles but in another configuration. In the case of scanning over the surface, the laser-beam is moving in respect to both the object and observer, repeatedly illuminating the object surface. Since this configuration differs from the classical one, the statistical properties of dynamic speckles have some specific features. Particularly, two sequential scans of the same rough surface result in the formation of two dynamic speckle patterns which are highly correlated in both time and space domains. After spatial filtering, highly correlated speckle patterns produce correlated photocurrents which have the same spectrum and the same shape. Therefore, any method for frequency estimation will result in the same constant value of measured frequency. Averaging the constants does not improve accuracy, and scanning over the same part of the object is useless.

To get uncorrelated photocurrent, either the object surface should be displaced in respect to the previous scan or the photodetector should be moved in respect to its position during the previous measurement. In both cases, either the speckle pattern is changed or the Ronchi rulings filters a new portion of dynamic speckles. Thus, the photocurrents become uncorrelated and averaging improves the accuracy. The minimal required displacements of the spatial filter and object surface to get independent measurements are termed *correlation parameters*. The first correlation parameter, L_{CD}, defines the distance on the object surface at which the adjacent scans should be displaced to result in uncorrelated responses of the photodiode. This parameter refers to the multi-scanning sensor operation mode. The second correlation parameter, L_{CP}, is the distance between two non-overlapped areas at the observation plane (at the plane of the spatial filter) situated so that the light collected from them into different photodiodes generates uncorrelated responses. This parameter refers to the multi-channel sensor mode. A detailed analysis of the correlation of spatially filtered dynamic speckles is given in **paper VI**. This section presents a general explanation and experimental estimation of speckle correlation phenomenon in the case of a SDS.

6.2 Multi-scanning sensor

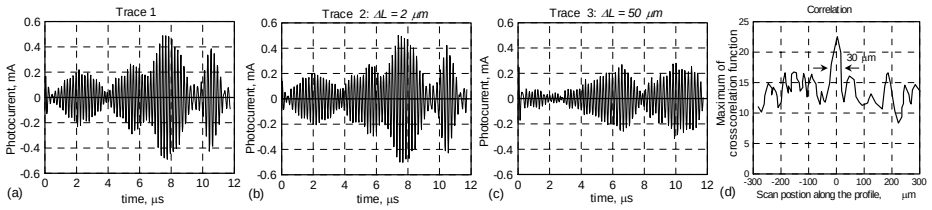

Figure 6.1. (a), (b), and (c) oscilloscope traces of the photocurrent for different displacements of the object surface perpendicular to the direction of the laser-beam scanning. (d) The maximum of cross-correlations calculated between a randomly selected scan and all others from the set of recorded data.

To study the correlation phenomenon, the standard scheme of the experimental setup was used (see Fig. 5.14). To demonstrate the correlation, the object under study was displaced a small distance and scanned again. Thereafter, the cross-correlation of the recorded photocurrent traces was calculated. The experiments were carried out with both transversal and longitudinal displacement of the object.

In this experiment, the light beam at the surface had an elliptical shape size of 600 μm in the direction of scanning and size of 60 μm in the orthogonal direction. Each subsequent scan was shifted 2 μm in respect to the previous one. By sequentially displacing the object surface orthogonally to the scanning beam, 2300 oscilloscope traces were recorded. Fig. 6.1(a,b,c) shows three typical responses from the recorded set of data. The surface was shifted 2 μm between the moments of recording traces 1 and 2, while the shift was 50 μm between traces 1 and 3. It can be seen that the shape of trace 2 is almost the same as that of trace 1 but trace 3 has a completely different shape from both the previous traces.

To estimate the correlation parameter L_{CD}, cross-correlation of a selected trace with all other traces was calculated. A typical result for one scan in the middle of the set is shown in Fig. 6.1(d). Here, zero in the abscissa axis is referred to as the scan position at the surface corresponding to the chosen trace. Repeating calculations of cross-correlations for differently chosen traces, it was found that the average width of the correlation peak was 30 μm. Given that the size of the illuminating beam in the direction of surface displacement is 60 μm, the correlated displacement is equal to r_B. The theoretical explanation for this is given in **paper VI**.

The experiment was repeated with different cylindrical lenses which allow the beam size in the direction orthogonal to scanning to be changed while keeping the other size the same (600 μm). With beam sizes of 400 and 1400 μm, the correlation parameter L_{CD} was equal to 200 and 700 μm, respectively, i.e. equal to r_B.
The correlation parameter L_{CD} in the case of longitudinal displacement of the surface (see **paper VI**) was found to be also equal to half of the full size of the illuminated spot at the surface, r_B.

6.3 Multi-channel sensor

In previous sections, the correlation properties of filtered dynamic speckles where measurements are performed by a single photodiode were discussed. However, there are many kinds of objects which provide light scattering in a wide solid angle while only a small part of the scattered light is collected into a photodiode. For example, with a metallic plate, which was used as a test object, only 0.15% of the reflected light power was spatially filtered and collected into the photodiode: the rest of the scattered light was not used. Installation of additional spatial filters and photodiodes, with averaging of their signals, would allow the distance measurement accuracy to be increased if the responses of these photodiodes are not correlated. This section presents the results of experimental study of the correlation properties of dynamic speckles when scattered and filtered light is collected into at least two photodiodes.

Many-channel spatial filtering is a very promising sensor performance improvement. However, it is clear that photodiodes located very closely to each other can produce correlated photocurrents. Therefore, identifying the minimal distance between adjacent photodiodes at which their responses are uncorrelated (correlation parameter defined above as L_{CP}) is very important for the proper location of photodiodes in a multi-channel sensor. Estimation of the correlation parameter L_{CP} is quite simple: the laser beam continuously scans a static object while the photodiode is displaced from point 1 to point 2 in the observation plane, as shown in Fig. 6.2(a).

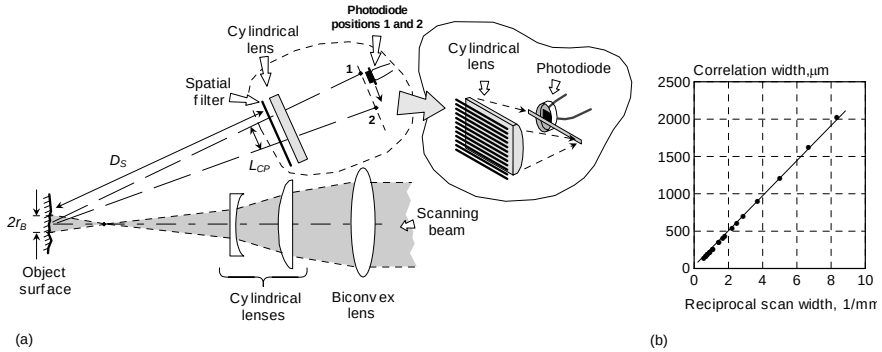

Figure 6.2. (a) Experimental setup for measuring the correlation length in a multi-channel dynamic-speckles sensor. Numbers 1 and 2 indicate adjacent positions of the photodiode at which its responses are uncorrelated, (b) Correlation length L_{CP} as a function of the reciprocal size $(2r_B)^{-1}$ of the scanning beam measured in a direction orthogonal to the scan. The red solid line is the average diameter of the speckles at the plane of the spatial filter.

The displacement of the photodiode is orthogonal to the direction of scanning. The photodiode aperture is 0.25 × 1.9, where the first size is measured along the direction of its displacement. Two cylindrical lenses were added in the illuminating part so that their axes were perpendicular to the plane of the drawing in Fig. 6.2(a). By varying their position it was possible to change the size of the scanning beam in a direction orthogonal to the scan while the other size was kept the same, since it is defined by the biconvex lens.

For each position of the cylindrical lenses in the illuminating arm, oscilloscope traces of the photocurrent at different positions of the photodiode were recorded. Cross correlations of the photodiode responses were calculated in a similar way as described for the multi-scanning sensor operation mode. Thereafter, the correlation parameter, L_{CP}, was estimated as a correlation-peak width. By repeating the measurements for different positions of the cylindrical lenses, the dependence of the correlation length L_{CP} on the beam size $2r_B$ was obtained, and it is shown in Fig. 6.2(b). As can be seen, in contrast with the multi-scanning operation mode, the correlation parameter, L_{CP}, is inversely proportional to the beam size. It is worth noting that the correlation displacement is equal to the mean speckle size, which is actually defined by the beam width, as reported in **paper VI**.

6.4 Discussion

Further increase in *z*-distance accuracy can be achieved by multiple scanning using multi-channel spatial filtering. In this case each subsequent scan should be shifted from the previous one by the distance of $L_{CD} = r_B$. Suppose that during scan number "*j*" the mean frequency of the photocurrent in the *i*-channel is measured to be $f_{PD_{ij}}$. If the total number of photodiodes is *N,* then after *M* scans over the object surface, the *z*-distance will be

$$\bar{z} = \frac{V_{BS}}{NM} \sum_{i}^{N} \sum_{j}^{M} \frac{D_{F_i}}{\Lambda_i f_{PD_{ij}} - V_{BS}} . \qquad (6.1)$$

Multiple scanning of the object surface can be readily implemented with continuously moving production lines. By scanning the surface in a direction orthogonal to the line movement, one can adjust the footprint width and scanning-repetition rate to the actual velocity of the line so that optimal covering of the surface with beam scans will be achieved. At the same time it is reasonable to use a single spatial filter with an array of photodiodes. In this case the footprint width at the surface defines the minimal distance between the photodiodes in the array to produce uncorrelated measurements.

On the basis of the experimental study of a single-photodiode dynamic-speckle sensor reported in **paper IV**, which estimates z-distance accuracy $\Delta z = 110$ μm for scan duration $t_{SC} = 2.5$ μs, it is feasible to design a 25-channel sensor capable of measuring distance with an accuracy of 1 μm in the time-window of 1 ms. In the next section, SDS performance is demonstrated; the necessity of taking the correlation phenomenon into account by using a scanning sensor is shown.

7 Demonstraation of speckle sensor performance

In all the above-mentioned experiments, including estimation of SDS accuracy, the test objects were made of metallic plates. The object surface was typically polished with a sandpaper to achieve light scattering in a smaller solid angle. At the same time, the test objects typically possessed high reflection power. Both high reflection power and small scattering angle allowed the collection of more photons to the photodiode and thus increasing the SNR. To demonstrate the functionality of a SDS with non-tailored objects, two experiments are presented in this section. The first experiment was made with a metallic tube and the target of measurement was a protective coating which was sprayed over the tube surface. Due to this coating, the reflection power of the surface was noticeably smaller than that of pure metallic objects. In addition, the light reflected from the coating was scattered uniformly into the spherical cap, which was almost equal to the hemisphere. The experiment was conducted in both a laboratory and a manufacturing environment. Thus, the first demonstration proves the feasibility of speckle ranging in actual operating conditions. The aim of the second experiment was to demonstrate that a SDS can work with non-metallic objects. In this experiment, a sheet of office paper was chosen as the test object. Both experiments and their results are presented below.

7.1 Profile measurement of protective coatings

Measurement of the thickness of protective coatings is a wide area of applications [1,50,51,52]. In this experiment the test object was a metallic tube with a diameter of 16 cm and lateral length of 20 cm. The profile of the tube was covered with a sprayed coating. The diameter of the tube was constant along the tube axis, and since the coating was sprayed non-uniformly the small variations (< 200 μm) in it correspond to the test profile. The aim of experiment was the measurement of the relative profile depth. The test object and the scheme of the experiment are shown in Fig 7.1.

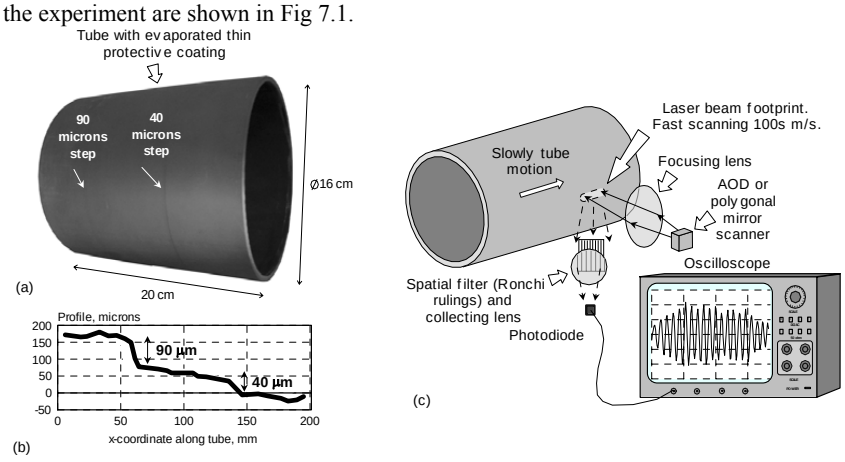

Figure 7.1. (a) A tube with a variable profile, (b) Profile of the tube measured using a conventional profiler, (c) Scheme of profile measurements using a SDS.

Fast scanning over the tube surface was implemented with an AOD. Scan duration of 20 μs provided a scanning rate of 50,000 per second. To measure the whole profile, the tube was slowly (relative to scanning velocity) moving in a direction parallel to the laser footprint. Each subsequent scan was displaced 4 μm,

while the beam radius was 300 μm and the footprint length was 1,100 μm. Thus, the sensor repeatedly scanned almost the same part of the tube surface many times, and the photocurrents acquired from adjacent scans correlated with each other. The whole tube profile (18 cm) was scanned within one second (net time), thus 50,000 traces of photocurrents were collected and saved to a digital oscilloscope. Thereafter, the collection of 50,000 traces was processed off-line with the MatLAB Signal Processing Toolbox. Each saved trace, *i*, was filtered with high- and low-pass filters. Then FFT was applied to each filtered trace *i* and after the FFT shape was approximated by a Gaussian function. The frequency corresponding to the maximum of the Gaussian function was taken as a mean frequency value of the photocurrent trace, f_{SPi}. Each frequency was recalculated to the sought distance *z* using Eq. 6.1. Thus, a collection of 50,000 measured *z*-distances was obtained. The results of profile measurements using the SDS are shown in Fig. 7.2, where they are compared with a profile measured with a conventional profilometer (solid lines). In each of the three charts of Fig. 7.2 the collection of 50,000 measured *z*-distances was processed in different ways to estimate data correlation:

a) The collection of 50,000 *z*-distances was averaged by 100 measurements. The 500 points obtained are displayed.
b) The collection of 50,000 *z*-distances was reduced to 2,000: only each 25th point was taken from the collection. The new collection of 2,000 points was averaged by 30 points, and these averaged 70 points are displayed.
c) The collection of 50,000 *z*-distances was averaged by 750 measurements. The 70 points obtained are displayed.

The most remarkable result of those calculations is that in case (a), despite using 100 averaging points, the dispersion of measurements is much stronger than in case (b), where each point on the chart is the result of averaging over only 30 points. This clearly proves that consideration of the correlation properties of speckles is of primary importance for the SDS. In case (a), 100 consequent points correspond only to 400 μm of scan displacement along the profile. Taking into account the scan length of 1,100 μm, this means that all 100 scans refer to almost the same part of the tube surface. Scanning of the same part of the surface resulted in highly correlated signals (as was shown in **paper VI),** and, therefore, the same measured frequency. Thus, averaging did not improve accuracy in case (a). At the same time, in case (b), in spite of the fact that only 30 scans were averaged, the distance between the first and last scan in the averaging sequence was 3,000 μm; thus, the correlation was less pronounced and, therefore, averaging appreciably improved the accuracy, in contrast to case (a).

Fig. 7.2(b,c) shows that the speckle sensor accurately measured the profile, and all small variations are clearly visible. The standard deviation calculated for the constant parts of the profile depth is equal to 2-7 μm (using data in Fig. 7.2(c): the profile acquired within 1 sec included all 50,000 measurements). This value is smaller than the surface roughness, which is 10-12 μm. In case (b), the net time of data acquisition of the whole tube profile was just 40 ms; however, the 40 μm step of the profile can easily be distinguished. By slightly increasing the measuring time, by using multi-channel filtering system, and taking into account the correlation phenomenon, one can easily achieve micron accuracy in the measurement of the protective coating thickness.

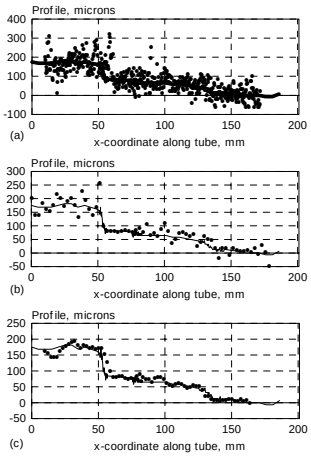

Figure 7.2. The solid line is a tube profile measured with a conventional profilometer; the points indicate the profile measured with a SDS: (a) The collection of 50,000 z-distances was averaged by 100 measurements. The 500 points obtained are displayed.; (b) The collection of 50,000 z-distances was reduced to 2,000: only each 25th point was taken from the collection. The new collection of 2,000 points was averaged by 30 points, and these averaged 70 points are displayed. (c) The collection of 50,000 z-distances was averaged by 750 measurements. The 70 points obtained are displayed.

Measurements to the test object (tube) were repeated on-line directly in a manufacturing environment with the compact prototype of the sensor, and were found to be feasible. However, due to the poor performance of the electronics (zero-crossing frequency meter), a measuring window of about several minutes was needed to distinguish the variation in the protective layer of 30 μm.

Analysis of the frequency measurement technique with the MatLAB showed that using zero-crossing with detection of bad mistakes instead of FFT slightly decreases accuracy. However, profile details can also be easily distinguished by applying zero-crossing to the collection of 50,000 measurements if the zero-crossing procedure detects and eliminates bad mistakes. At the same time, zero-crossing is considerably faster and is expected to be preferable for the multi-channel sensor.

7.2 Paper thickness measurements

The test objects in all the experiments described above were metallic surfaces: aluminium, iron, steel etc. To prove that the dynamic speckle method works with other rough surfaces, the method was tested with paper. Recently the first on-line system for paper thickness measurement using triangulation was demonstrated [53]. Here it is demonstrated that the SDS can measure paper thickness as well [52]. Measurement of paper thickness by means of speckles is quite difficult because illuminating light penetrates inside the paper and the formation of the speckle pattern is a result of light scattering from many different paper layers. The thickness of office paper is typically limited to 100 μm. Therefore, the speckle pattern contains information not only about the upper layer of the paper but about all the other layers inside.

To check the possibility of measuring distance to the paper, a sheet of standard office paper was fixed on the micro-translation stage to change the *z*-coordinate of the object. In the experiment the distance to the paper was varied in the range of 7-15 mm from the beam waist position with a step of 1 mm. The modulation frequency measured for each paper position was recalculated into the *z*-distance. The results were averaged over 5 scans. Scanning velocity was 20 m/s while the single scan duration was 250 μs.

Fig. 7.3 shows a schematic drawing of the light scattering (a) from a metallic surface, and (b) from paper. The respective modulated photocurrents are shown in Fig. 7.3(c,d). The SNR in modulation produced by paper is lower; however, its frequency can still be measured precisely. In Fig. 7.4(a) the Fourier transforms calculated for the modulated photocurrents acquired from the metal and the paper are compared. Both photocurrents were recorded when the test objects were located at the same *z*-distance. In spite of the fact that the Fourier peak with the paper is smaller than with the metal, the modulation frequency for both materials is the same. The results of distance measurements to the paper are shown in Fig. 7.4(b). Here the position of the paper sheet is estimated using the speckle method for the displacement 7-15 mm. The accuracy of the measurements was calculated as a standard deviation and it is within [300-1,000] microns. The dependence of the frequency on the *z*-coordinate is shown in Fig. 7.4(c). For all object positions except very close to the focus, the experimental dependence is well in accordance with the theoretical one.

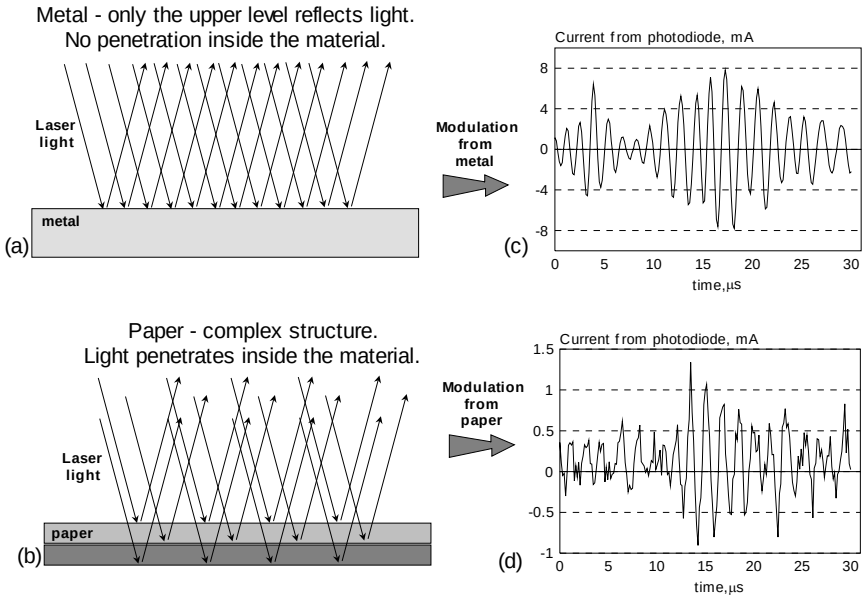

Figure 7.3. (a) Light scattering from the metallic surface, (b) light scattering from the paper, (c) modulation of photocurrent produced by the metal, (d) modulation of photocurrent produced by the paper.

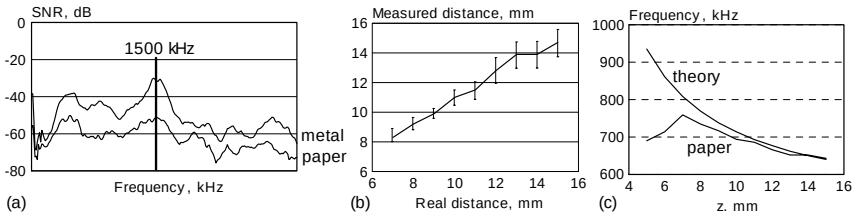

Figure 7.4. (a) FFT of photocurrents (upper line - metal, lower line - paper), (b) measured *z*-coordinate of the paper sheet using a SDS, (c) frequency dependence upon *z*-coordinate.

In spite of a poor accuracy of 300-1,000 μm, which is far beyond the requirements of the paper industry, the experiment showed that in principle it is possible to measure the thickness of papery objects using dynamic

speckles. The author would like to underline that the experiments with paper did not take place in optimal conditions: the scanning velocity was low, the same part of the object surface was scanned, and the correlation phenomenon was not taken into account.

It is expected that using a faster scanner and multi-channel spatial filtering will greatly improve the accuracy of paper measurements, while keeping a reasonably short response time.

8 Conclusion

In this thesis a novel approach for distance measurement using dynamic speckles is demonstrated. The possibility of using dynamic speckles for measuring the distance to moving objects has been known since the 1970s. The arrangement of a speckle distance sensor is as follows: the distance between the moving object and the illuminating laser defines the speckle velocity at the observation plane; the speckle velocity is measured by means of spatial filtering. In spite of the simple arrangement, speckle distance sensing does not attract enough attention among researchers and sensor manufacturers. In the opinion of the author, the reason for this is the short dynamic range expected for the speckle method. That is because the speckle measurement range is limited by several centimetres. In the case of a centimetre scale range, micron accuracy of measurement is required to achieve an acceptable dynamic range of the sensor. However, providing micron accuracy is quite a challenging task for a speckle sensor. The stochastic nature of speckles results in high dispersion of measurements and therefore low accuracy. The accuracy of the measurements can still be improved but at the expense of the measuring window. Acceptable accuracy can be achieved for measuring windows greater than 1 second. The long response time nullifies all the advantages of the method because conventional touch sensors perform better.

In this thesis it is demonstrated that the response time of the dynamic speckle method is defined mainly by the velocity of the test object. When illuminated with a laser beam the test object generates dynamic speckles. If the object moves faster, the velocity of the generated speckles rises. Fast speckles reduce the measurement response time and, therefore, more measurement results are accumulated within the same time window, and it is possible to increase the accuracy by means of averaging. Object velocities in a visual environment are limited typically to several meters per second. Low object velocity cannot provide a short enough response time to implement averaging within a reasonably short time window. This thesis proposes that fast scanning over the object surface improves the dynamic speckle ranging performance. Modern scanners provide scanning velocities of hundreds of meters per second. This is much faster than the movement of typical industrial objects. Rapid scanning greatly reduces the response time of the speckle sensor. Fast response allows the accumulation of more measurements results within a short time window and the use of averaging. Averaging provides micron accuracy of the speckle sensor; therefore, the dynamic range of the sensor becomes suitable for various ranging applications, as is demonstrated in this thesis. Scanning over the object is an important approach for ranging also because it allows measurements to be made to static objects, which was previously completely impossible.

Scanning techniques are now well-developed. Two fast scanners, an acousto-optic deflector and polygonal mirror scanner, are considered in the thesis. Several different models of both scanner types were extensively studied, and optimal parameters for each were identified.

Using an optimized speckle distance sensor, the trade-off between accuracy and sensor response was found to be 100 μm within a time window of just 2.5 μs. According to the statistical law, averaging over a longer time window increases the accuracy. Thus, for a time window of 25 ms one can achieve 1 μm accuracy and obtain the sensor dynamic range of at least 1,000:1 within 1 mm. It is worth noting that in addition to fast and accurate measurements, the speckle sensor can provide measurements to

- extremely rough objects where alternative methods decrease performance or even unable to operate
- fast-moving objects (tens m/s), as the scanning velocity is much faster (hundreds m/s)

Improving the performance of a dynamic speckle sensor requires knowledge of the correlation properties of dynamic speckles. Whereas the correlation properties of speckles produced by moving objects have been extensively studied, the correlation properties of spatial filtered speckles generated with scanning laser beam were studied for the first time in this thesis. Revealed correlations properties allow developing many-channel speckle distance sensor, which uses several photodiodes simultaneously. Averaging data from several channels allows increase accuracy without impairing response. For example, photodiode array size of 25 allows getting 1-μm accuracy within 1 ms.

The sensor performance was tested with various types of materials (metals, papers, etc.) and not only with tailored objects in laboratory conditions but also with object taken from industrial environment. As an example, the protective coating of the tube (length of 18 cm) was measured within just 1 second with accuracy of 2-7 μm which is higher then the object coating roughness 10-12 μm. The experiment was repeated during coating spraying over the tube surface in manufacturing environment where the sensor demonstrated also good performance.

The future work with sensor prototype requires some improvements and optimisations. The main optimization concerns development of optimal electronics for real time data processing. The most of data processing procedures during sensor testing were made off-line with a personal computer. Required electronics should measure frequencies of tens of megahertz continuously; it should take into account intermittent nature of an acquired signal, be able to eliminate bad mistakes and implement averaging. However, this seems to be not a complicated problem because zero-crossing method perfectly copes with frequency measurement. Zero-crossing method is not resource-intensive and can be easily realised with modern electronics even in case of multi-channel sensor.

Conducted research found the way to improve performance of dynamic speckle ranging technique, which to the opinion of the author was undeservingly neglected. Developed speckle ranging method demonstrated high accuracy and short response. High performance of the sensor was also corroborated by testing the sensor prototype in manufacturing environment. Author asserts that supplemented with appropriate electronics the sensor can find a lot of applications. Especially it concerns strongly scattering and fast moving objects where other techniques do not provide requited performance.

Appendix A

Principle of scanning with acousto-optic and polygonal mirror deflectors.

An acousto-optic deflector (AOD), also called a Bragg cell, uses the acousto-optic effect to change the angular position of laser beam propagating through the aperture of the deflector [44,43]. Acousto-optic deflection is based on changing the frequency of an acoustic wave, f_{ac}, activated in an acousto-optic crystal to vary the laser beam diffraction angle, Θ. Laser beam angular position is linearly proportional to the acoustic frequency, so that the higher the frequency, the larger the diffracted angle

$$\Delta\Theta \approx \lambda \cdot \frac{\Delta f_{ac}}{V_a} \qquad \text{(A.1)}$$

where λ is optical wavelength, V_a is the acoustic velocity, and Δf_{ac} is the acoustic wave frequency band. The scheme of diffraction in AOD is shown in Fig. A1.

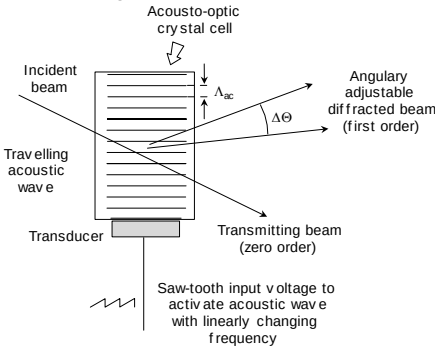

Figure A1. Scheme of laser beam diffraction in AOD.

The activated acoustic wave varies refractive index inside an acousto-optic cell along its propagation direction thus forming a diffraction grating with the period of $\Lambda_{ac} \sim 1/f_{ac}$. The acoustic wave is induced by the piezoelectric transducer bonded to the crystal. The angular position of the diffracted laser beam is linearly proportional to the frequency of generated acoustic wave. By applying a saw-tooth waveform to the AOD-driver, the acoustic waves with swept frequency is excited in AOD thus providing scanning of the surface by the laser beam.

Optimal position of AOD in the speckle sensor is in the focal point of the focusing lens as it is shown in Fig. A2. In this case the scanning beam moves perpendicularly to the object surface and *z*-distance between the optical head and the object is kept the same for any points in the scan. This also means that the modulation frequency does not change along the scan. This greatly simplifies measurement procedure. In the case of noticeable displacement of AOD from the focal point, *z*-distance between the lens and the object can be appreciably changing along the scan. Thus the modulation frequency, which is a function of *z*-distance, can be changing greatly along the scan. If *z*-distance changes too fast along the scan, the modulation can be even not observed.

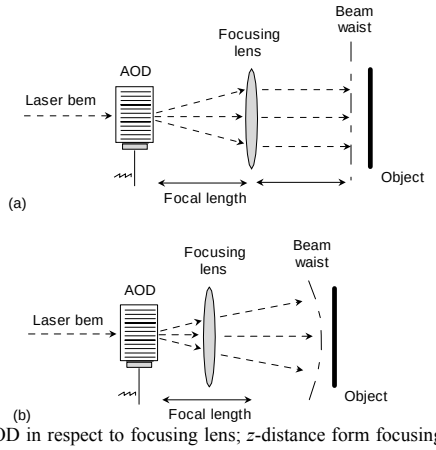

Figure A2. (a) Optimal position of AOD in respect to focusing lens; *z*-distance form focusing lens to the object is the same for any angular positions of scanning beam. (b) not optimal position of AOD in respect to focusing lens.

Optimal position of focusing lens results in a simple dependence of the scan length, L, on the maximal scanning angle, 2β, the focal length of the focusing lens, f_o, and the diameter of the lens, see Fig. A3. It is worth noting that the optimal position of the focusing lens in the case of the polygonal mirror scanner located before the focusing lens is the same as for AOD.

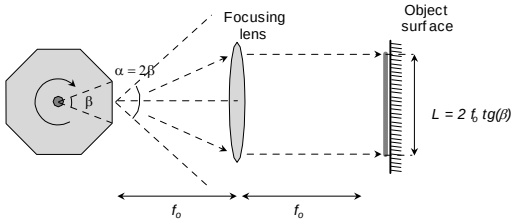

Figure A3. The Scan length, L, in the case of the optimal scanner position as a function of the scanning angle, 2β, the focal length, f_o, and the diameter of the lens.

Here the scan length is equal to $L = 2 \cdot fo \cdot tg(\beta)$. In the most of the experiments f_o = 50 mm. The use of the lenses with different focal lengths changes the scan length and therefore, the scanning velocity. However, using lens with a longer focal length in spite of the higher scanning velocity does not increase the modulation frequency, which is expected according to Eq. 4.8. This is because the lens with a longer focal length reduces the numerical aperture of the illuminating beam and the numerical aperture is the crucial parameter, which defines the maximal achievable frequency, see Eq. 5.7

In this thesis two different AOD were utilized with 1.5° and 1.8° angular band. Both AODs were manufactured in Scientific Instruments, Ltd., Russia and their parameters are listed in table A1. The focal length of 50 mm and given angular bandwidths results in scan size of 1.3 and 1.6 mm (which is in accordance with experimental estimations 1.1 and 1.5, respectively). For the polygonal mirror scanner the angular band is not limited as for AOD and it is defined by the number of facets of the mirror, n, because $\alpha = 360 \cdot 2/n$, see Fig. A3. Therefore, the scan length in the case of the polygonal mirror scanner can be much longer. For the 8-facets mirror α = 90° and the respective scan length is 100 mm. Parameters of 8- and 72-facets mirror scanners are given in the table A2.

Appendix A

Table A1. Parameters of acousto-optic deflectors.

AOD	Acousto-optic crystal	Acoustic wave velocity (m/s)	Angular band (degrees)	Minimal scan duration (μs)	Scan length (mm)	Acoustic wave frequency band (MHz)	Diffraction efficiency (%)	Scanning velocity (m/s)
Slow	TeO_2 [110]	690	1.8	10 - 20	1.6	60 - 100	80	>100
Fast	TeO_2 [001]	4200	1.5	2 - 4	1.3	275 - 450	10	> 500

Table A2. Polygonal mirror deflector parameters.

Number of facets	Angular band (degrees)	Minimal scan duration for 30,000 rpm (μs)	Scan length (mm)	Scanning velocity (m/s)
8	90	250	100	~ 400
72	10	28	8.7	~ 320

From tables A1 and A2 one can see that the scanning velocity with polygonal scanners is the same order of value as with the AODs. Polygonal scanner has about 10 times longer duration of the scan but it is compensated by the length of the scan.

References

[1] Nadeau, A., Pouliot, L., Nadeau, F., Blain, J., Berube, S. A., Moreu, C., and Lamotagne, M. (2006) A new apoproach to online thickness measurements of thermal spray coatings. Proceedings of the 2006 International Thermal Spray Conference, Seatle, Washington, USA.

[2] Yamaguchi, I., Komatsu, S., and Saito, H. (1975) Dynamics of speckles produced by a moving object and its applications. Japanese Journal of Applied Physics, Part 1: 14, 301-306.

[3] Yamaguchi, I. and Komatsu, S. (1977) Theory and applications of dynamic laser speckles due to in-plane object motion. Optica Acta 24, 705-724.

[4] Giglio, M., Musazzi, S., and Perini, U. (1981) Distance measurement from a moving object based on speckle velocity detection. Applied Optics 20, 721-722.

[5] Aizu, Y. and Asakura, T. (2006) Spatial Filtering Velocimetry: Fundamentals and Applications. Springer.

[6] Pusey, P. N. (1976) Photon correlation study of laser speckle produced by a moving rough surface. Journal of Physics D: Applied Physics 9, 1399-1409.

[7] Aizu, Y. and Asakura, T. (1987) Principles and development of spatial filtering velocimetry. Applied Physics B-Photophysics and Laser Chemistry 43, 209-224.

[8] Hayashi, A. and Kitagawa, Y. (1982) Laser speckle velocimeter utilizing optical fibers. Optics Communications 43, 161-163.

[9] Hayashi, A. and Kitagawa, Y. (1982) Image velocity sensing using an optical fiber array. Applied Optics 21, 1394-1399.

[10] Asakura, T. and Takai, N. (1981) Dynamic laser speckles and their application to velocity measurements of the diffuse object. Applied Physics 25, 179-194

[11] Bosch J.A. (1995) Coordinate Measuring Machines and Systems. Dekker, New York.

[12] Jagiella M., Fericean S., Droxler R., and Albert D. (2005) New Magneto-inductive Sensing Principle and its Implementation in Sensors for Industrial Applications. Techniches Messen 72(11), 622-631.

[13] Bury, B. (1991) Proximity sensing for robots. Robot Sensors, IEE Colloquium on 3/1-318.

[14] Trдnkler H.R. and Obermeier E. (1998) Sensortechnik. Springer, Berlin.

[15] Biber C., Ellin S., Stempeck J., and Sheck E. (1980) The Polaroid ultrasonic ranging system. In 67th Audio Engineering Society Convention.

[16] Strand, T. C. (1985) Optical three-dimension sensing for machine vision. Optical Engineering 24, 33-40.

References

[17] Lewis R.A. and Johnson A.R (1977) A Scanning Laser Rangefinder. for a Robotic Vehicle. Proceedings Robots 3 762-768.

[18] Zheng J. (2005) Optical Frequency-modulated Continuous-wave (FMCW) Interferometry. Springer, Germany.

[19] Nitzan D., Brain A.E., and Duda R.O (1977) The measurements and use of registered reflectance and range data in scene analysis. Proc.IEEE 65, 206-220.

[20] Penney C.M. and Thomas B. (1989) High performance laser triangulation. J.of Laser Applications 1-58.

[21] Yamaguchi, I. (1980) Real-time measurements of in-plane translation and tilt by electronic speckle correlation. Japanese Journal of Applied Physics, 19, L133.

[22] Ohtsubo, J. and Asakura, T. (1975) Statistical properties of speckle intensity variations in the diffraction field under illumination of coherent light. Optics Communications 14, 30-34.

[23] Takai, N. and Asakura, T. (1985) Vectorial measurements of speckle displacement by the 2-D electronic correlation method. Applied Optics 24, 660-666.

[24] Sirohi R.S. (1993) Speckle Metrology. Marcel Dekker Inc.

[25] Yamaguchi, I. (1985) Fringe formations in deformation and vibration measurements using laser light. Progress in Optics 22, 174-341.

[26] Archbold E., Burch J.M., and Ennos A.E. (1970) Recording of in-plane surface displacement by double-exposure speckle photography. Optica Acta 17, 883-898.

[27] Tiziani, H. J. (1971) Application of speckling for in-plane vibration analysis. Optica Acta 18, 891-902.

[28] Tiziani H.J. (1972) A study of the use of laser speckles to measure small tilts of optically rough surfaces. OPT COMMUN 5, 271-274.

[29] Peters W.H and Ranson W.F. (1982) Digital imaging techniques in experimental stress analysis. Optical Engineering 21, 427-431.

[30] Yoshimura, T. (1986) Statistical properties of dynamic speckles. Journal of the Optical Society of America A-Optics and Image Science 3, 1032-1054.

[31] Ator, J. T. (1963) Image-velocity sensing with parallel-slit reticles. J.Opt.Soc.Am. 53, 1416-1422.

[32] Gaster, M. (1964) A new technique for the measurement of low fluid velocities. Journal of Fluid Mechanics 20, 183-192.

[33] Durst F., Melling A., and Whitelaw J.H. (1976) Principles and Practice of Laser-Doppler Anemometry . Academic Press, London.

[34] Durrani T.S. and Greated C.A. (1977) Laser Systems in Flow Measurement . Plenum Press, New York.

[35] Drain L.E. (1980) The Laser Doppler Technique . John Wiley & Sons, Chichester.

[36] Mishina H., Ushizaka T., Tokui S., Asakura T., and Nagai S (1975) A Laser Doppler Microscope : Its Signal-Analyzing Systems : Doppler Velocimetry. Jpn.J.Appl.Phys.Suppl. 14, 323-328.

[37] Riedel, K. S. (1994) Kernel estimation of the instantaneous frequency. IEEE Trans.on Signal Processing 42, 2644-2649.

[38] Brigham E.O. (1974) The Fast Fourier Transforms. Prentice-Hall, New Jersey.

[39] Bracewell R.N. (1978) The Fourier Transforms and its Applications International Student Edition. McGraw-Hill Kogakusha, Tokyo.

[40] Veselov, L. M. and Popov, I. A. (1998) Statistical properties of modulated dynamic speckles. Opt.Spectrosc. 84, 268-272.

[41] Takai, N., Iwai, T., Ushizaka, T., and Asakura, T. (1980) Zero-crossing study on dynamic properties of speckles. J.Opt.(Paris) 11, 93-101.

[42] Sherman R J (1988) Comparing beam-deflecting systems. Photonic Spectra 22(3), 89-90.

[43] I.C.Chang (1976) Acousto-optic Devices and Applications. IEEE Transactions on Sonics and Ultrasonics SU-23(1), 2-22.

[44] Yariv, A. and Yeh, P. (1984) Optical waves in crystals. Wiley, New York.

[45] Dickson L.D. (1972) Optical considerations for an acoustooptic deflector. Applied Optics 11, 2196-2202.

[46] Rigden, J. D. and Gordon, E. I. (1962) The granularity of scattered optical maser light. Proc.IRE 50, 2367-2368.

[47] Oliver, B. M. (1963) Sparkling spots and random diffraction. Proc.IEEE 51, 220-221.

[48] Stavis, G. (1966) Optical diffraction velocimeter. Instruments & Control Systems 39, 99-102.

[49] Komatsu, S., Yamaguchi, I., and Saito, H. (1976) Velocity measurements using structural change of speckle. Optics Communications 18, 314-316.

[50] Davis, R. D. (2004) Handbook of Thermal Spray Technology. ASM international.

[51] Kamshilin, A. A., Semenov, D. V., Nippolainen, E., and Miridonov, S. V. (2007) Dynamic-speckle profilometer for online measurements of coating thickness. Journal of Physics: Conference Series 85, 012021-1-012021-6.

[52] Semenov, D. V., Nippolainen, E., and Kamshilin, A. A. (2005) Measurements of paper thickness by use of dynamic speckles. Technical Digest of Sixth Japan-Finland Joint Symposium on Optics in Engineering, Sapporo, 67-68.

[53] Graeffe, J. and Nuyan, S. (2005) An online laser caliper measurement for the paper industry. SPIE 5856, 318-326.

Kuopio University Publications C. Natural and Environmental Sciences

C 208. Anttonen, Mikko J. Evaluation of Means to Increase the Content of Bioactive Phenolic Compounds in Soft Fruits.
2007. 93 p. Acad. Diss.

C 209. Pirkanniemi, Kari. Complexing agents: a study of short term toxicity, catalytic oxidative degradation and concentrations in industrial waste waters.
2007. 83 p. Acad. Diss.

C 210. Leppänen, Teemu. Effect of fiber orientation on cockling of paper.
2007. 96 p. Acad. Diss.

C 211. Nieminen, Heikki. Acoustic Properties of Articular Cartilage: Effect of Structure, Composition and Mechanical Loading.
2007. 80 p. Acad. Diss.

C 212. Tossavainen, Olli-Pekka. Shape estimation in electrical impedance tomography.
2007. 64 p. Acad. Diss.

C 213. Georgiadis, Stefanos. State-Space Modeling and Bayesian Methods for Evoked Potential Estimation.
2007. 179 p. Acad. Diss.

C 214. Sierpowska, Joanna. Electrical and dielectric characterization of trabecular bone quality.
2007. 92 p. Acad. Diss.

C 215. Koivunen, Jari. Effects of conventional treatment, tertiary treatment and disinfection processes on hygienic and physico-chemical quality of municipal wastewaters.
2007. 80 p. Acad. Diss.

C 216. Lammentausta, Eveliina. Structural and mechanical characterization of articular cartilage and trabecular bone with quantitative NMR .
2007. 89 p. Acad. Diss.

C 217. Veijalainen, Anna-Maria. Sustainable organic waste management in tree-seedling production.
2007. 114 p. Acad. Diss.

C 218. Madetoja, Elina. Novel process line approach for model-based optimization in papermaking.
2007. 125 p. Acad. Diss.

C 219. Hyttinen, Marko. Formation of organic compounds and subsequent emissions from ventilation filters.
2007. 80 p. Acad. Diss.

C 220. Plumed-Ferrer, Carmen. Lactobacillus plantarum: from application to protein expression.
2007. 60 p. Acad. Diss.

C 221. Saavalainen, Katri. Evaluation of the mechanisms of gene regulation on the chromatin level at the example of human hyaluronan synthase 2 and cyclin C genes.
2007. 102 p. Acad. Diss.

C 222. Koponen, Hannu T. Production of nitrous oxide (N□O) and nitric oxide (NO) in boreal agricultural soils at low temperature.
2007. 102 p. Acad. Diss.